DISCLAIMER NOTICE

THIS DOCUMENT IS BEST QUALITY PRACTICABLE. THE COPY FURNISHED TO DTIC CONTAINED A SIGNIFICANT NUMBER OF PAGES WHICH DO NOT REPRODUCE LEGIBLY.

(1)

DS/ME/75-2

A MODEL FOR FLUORINE RECOMBINATION AT A METAL SURFACE

by

Eric J. Jumper, B.S., M.S.
CAPT USAF

Approved:

Chairman	8 Dec 75
	31 Dec 75
	8 Dec 75
	9 Dec 1975

Accepted:

Dean, School of Engineering	9 Dec 1975

DS/ME/75-2

A MODEL FOR FLUORINE RECOMBINATION AT A METAL SURFACE

DISSERTATION

Presented to the Faculty of the School of Engineering
of the Air Force Institute of Technology
Air University
in Partial Fulfillment of the
Requirements for the Degree of
Doctor of Philosophy

by

Eric J. Jumper, B.S., M.S.

Approved for public release; distribution unlimited.

ia

UNCLASSIFIED

SECURITY CLASSIFICATION OF THIS PAGE (When Data Entered)

REPORT DOCUMENTATION PAGE	READ INSTRUCTIONS BEFORE COMPLETING FORM
1 REPORT NUMBER: DS/NE/75-2	2 GOVT ACCESSION NO	3 RECIPIENT'S CATALOG NUMBER
4 TITLE (and Subtitle): A MODEL FOR FLUORINE RECOMBINATION AT A METAL SURFACE	5 TYPE OF REPORT & PERIOD COVERED: Ph.D. Dissertation 6 PERFORMING ORG. REPORT NUMBER
7 AUTHOR(s): Eric J. Jumper, Capt	8 CONTRACT OR GRANT NUMBER(s)
9 PERFORMING ORGANIZATION NAME AND ADDRESS: Air Force Institute of Technology (AFIT/EN), Wright-Patterson AFB, Ohio 45433	10 PROGRAM ELEMENT, PROJECT, TASK AREA & WORK UNIT NUMBERS
11 CONTROLLING OFFICE NAME AND ADDRESS: Air Force Weapons Laboratory (AFWL/DYT), Kirtland AFB, New Mexico 87117	12 REPORT DATE: December 1975 13 NUMBER OF PAGES: 222
14 MONITORING AGENCY NAME & ADDRESS (if different from Controlling Office)	15 SECURITY CLASS (of this report): UNCLASSIFIED 15a DECLASSIFICATION/DOWNGRADING SCHEDULE

16 DISTRIBUTION STATEMENT (of this Report)

Approved for public release; distribution unlimited.

17 DISTRIBUTION STATEMENT (of the abstract entered in Block 20, if different from Report)

18 SUPPLEMENTARY NOTES

Approved for public release; IAW AFR 190-17

JERRY C. HIX, Captain, USAF
Director of Information

19 KEY WORDS (Continue on reverse side if necessary and identify by block number)

Heterogeneous Recombination
Fluorine Recombination
Chemical Laser
Chemical Laser Nozzle Flow
Catalytic Fluorine Recombination
Wall Recombination
Viscous Nozzle Flow

20 ABSTRACT (Continue on reverse side if necessary and identify by block number)

A steady state model for fluorine atom recombination for temperatures less than 800 K on a metal catalytic surface was developed based on the Rideal heterogeneous reaction mechanism. The model is comprised of three distinct processes: (1) the bonding process of gas-phase fluorine atoms to the metal surface, (2) the collision and subsequent recombination process of gas-phase atoms and surface-bonded fluorine atoms and (3) the rate process at which the bonding and recombination take place consider-

DD FORM 1473 EDITION OF 1 NOV 65 IS OBSOLETE

UNCLASSIFIED

SECURITY CLASSIFICATION OF THIS PAGE (When Data Entered)

ing the surface coverage. The model was compared with actual fluorine recombination data taken for a nickel tube in which a gas mixture of atomic fluorine, molecular fluorine, and argon flowed. The results of this comparison validated the model and extended the verification of the Rideal mechanism for heterogeneous recombination.

Computations using the wall recombination model were made for a two-dimensional slit nozzle of the type used in fluorine chemical lasers, using a two-dimensional chemically reacting laminar boundary layer computer code. The results of these computations showed that the wall recombination substantially affected the temperature profiles as well as wall heat transfer in chemical laser nozzles. The amount of atomic fluorine depleted through wall recombination was shown to be on the order of a third of the initial fluorine concentration for the nozzle configuration run.

Preface

The origin of this dissertation dates back to a trip I made to the Weapons Laboratory in March 1973. At that time the problem of fluorine recombination seemed to me to be an extremely pressing one, and one which I thought would certainly be solved by the time I was ready to begin my research. I returned to AFIT and began to prepare myself for embarking on a parametric study of heat transfer effects due to fluorine recombination on the walls of the small nozzles in a fluorine chemical laser using someone else's recombination model (which I assumed would be in existence when I needed it).

While I was back at AFIT, an interesting thing took place in fluorine chemical laser circles. It was the discovery of the infamous "Hot Chain" fluorine laser reaction. In effect the Hot Chain was advertised as being able to produce excited HF and DF using a reaction which required only small amounts of atomic fluorine and large amounts of molecular fluorine. The effect of this "discovery" was to put an end to the urgency of developing a fluorine wall recombination model. Thus, by the time I arrived at the Weapons Laboratory to begin my parametric study, nothing had been done on developing a recombination model. The model was still considered an interesting problem but no longer an urgent one. So, I began the work of developing

the recombination model presented here. In the same time frame some of the early tests using the Hot Chain were being undertaken with negative results but high hopes.

About six months ago people began to realize that the Hot Chain was not all it had been assumed to be. Suddenly, wall recombination was again an important and pressing problem and I had people asking for my model. In this regard, I found the work most exciting, especially since, because of the time involved in performing the research, most dissertation topics are not of such immediate importance. So, as I begin thanking those individuals who aided me in my work, I would first like to thank whoever it was who first suggested that the answer to fluorine wall recombination was the Hot Chain.

In all seriousness, I would like to thank all those at the Weapons Laboratory who were of such help to me, in particular, LtCol Jay Roland, LtCol David Ericson, Maj Dick Harris, a special thanks to LtCol Dick Roberds for his patient ear, and, certainly not least, Mrs Esther Caster for typing this dissertation. I am also indebted to several members of the AFIT faculty, in particular, my advisor Dr James Hitchcock for his helpful suggestions and comments and Dr Andrew Shine for his confidence in me.

I would like to express a very special thanks to Dr Casper Ultee of United Aircraft Research Laboratory for

graciously making his previously unpublished data available to me for this study.

Finally, to my wife Marge and my children John and Christy I want you to know how thankful I am for your constant love, understanding and sacrifice over the long three years since I began work on my PhD. To you three I dedicate this dissertation.

Eric J. Jumper

Contents

Contents

List of Figures

List of Figures

List of Tables

List of Symbols

C_a	Surface sites per unit area
c_p	Specific heat at constant pressure
$\mathcal{D}$	Diffusivity
D	Well depth
E_D	Desorption energy
F_i	Mole-mass ratio of species i (moles-g_{mix}^{-1})
h	Planck constant
$\hbar$	Planck constant divided by 2π
h_i	Enthalpy of species i
k	Thermal conductivity
k_i	Thermal conductivity of species i
K_b	Backward rate constant
K_f	Forward rate constant
k	Boltzmann constant
k_g	Gas-Wall spring constant
k_s	Surface spring constant
m	Mass of atom
$\dot{N}$	Rate of impingement
n	Volumetric or surface number density
P	Pressure
q	Orbital radius of electrons of atom times charge
R	Universal gas constant
R_E	Equilibrium position
r	Position or pipe radius depending on context

List of Symbols

S	Sticking coefficient
S_o	Clean surface sticking coefficient
S_t	Steric factor
T	Temperature
t_c	Time of collision
t_{DIFF}	Characteristic time of diffusion
t_{REC}	Characteristic time of recombination depletion
U	Flow velocity
u	X-component of velocity
V	Velocity
$V(r)$	Repulsive potential
$V_{1,2,3}$	Velocity components on atomic scale
v	Y-component of velocity
$\bar{v}$	Mean atomic velocity
$W(r)$	Attractive potential
$\dot{W}_i$	Rate of production of species i
x	Longitudinal position
$\tilde{x}$	Axial position
Y	Position of gas atom
$\dot{Y}$	Velocity of gas atom
y	Transverse position
Z	Position of surface atom
$\dot{Z}$	Velocity of surface atom

List of Symbols

γ	Recombination coefficient
δ	Thermal desorption
ΔE_w	Well depth
ϵ	Maximum energy of attraction between colliding atoms
θ	Surface coverage ratio
κ	Interaction distance
λ	Mean free path
μ	Viscosity
σ	Cross section
χ	Mole fraction
Ω	Reduced collision integral
ω	Frequency

Subscripts

D	Diluent or diffusion depending on context
F	Fluorine
T	Total
o	Initial
i	Species i
g	Gas
s	Surface
μ	Viscosity

Abstract

A steady state model for fluorine atom recombination for temperatures less than 800 K on a metal catalytic surface was developed based on the Rideal heterogeneous reaction mechanism. The model is comprised of three distinct processes: (1) the bonding process of gas-phase fluorine atoms to the metal surface, (2) the collision and subsequent recombination process of gas-phase atoms and surface-bonded fluorine atoms and (3) the rate process at which the bonding and recombination take place considering the surface coverage. The model was compared with actual fluorine recombination data taken for a nickel tube in which a gas mixture of atomic fluorine, molecular fluorine, and argon flowed. The results of this comparison validated the model and extended the verification of the Rideal mechanism for heterogeneous recombination.

Important characteristics of fluorine wall recombination were demonstrated through use of the model. The recombination coefficient, defined as the ratio of the recombination resulting wall collisions to the total wall collisions, was found to be a strong function of temperature. The recombination coefficient dropped rapidly from a maximum of approximately 10^{-2} at 400 K to approximately 3×10^{-6} at 700 K due to thermal desorption. The

recombination coefficient was also found to be strongly dependent on the diluent of the gas mixture for lower temperatures. An argon diluent was found to greatly limit the recombination coefficient at temperatures below 400 K. Helium is predicted to have much less of a limiting influence when used as a diluent.

Computations using the wall recombination model were made for a two-dimensional slit nozzle of the type used in fluorine chemical lasers, using a two-dimensional chemically reacting laminar boundary layer computer code. The results of these computations showed that the wall recombination substantially effected the temperature profiles as well as wall heat transfer in chemical laser nozzles. The amount of atomic fluorine depleted through wall recombination was shown to be on the order of a third of the initial fluorine concentration for the nozzle configuration run.

A MODEL FOR FLUORINE RECOMBINATION AT A METAL SURFACE

I. Introduction

Background

For some years now it has been known that chemical lasers have a much higher performance potential than gas dynamic lasers, GDL, in terms of volumetric efficiency, chemical efficiency, and gain (Ref 1). Because of the simpler technology involved, GDL's were the first lasers to be explored at the development level for the production of a high power laser. Research, however, has continued on chemical lasers to lay the ground work for the second generation of high power lasers. Since 1971 considerable effort has been expended in the production of comprehensive gasdynamic computer models for the study and design of chemical lasers (Ref 2).

Computer modeling of the nozzle banks, lasing cavities and diffusor sections is just beginning to gain acceptance. Usable results are beginning to be produced toward the final goal of merging the separate models of each of the components into an overall design code. Of major importance to these codes are the physiochemical inputs. These inputs are presently being looked at in great detail in an attempt to further refine the semi-empirical models.

One area which has been in question for a number of years is that of the fluorine wall recombination reaction in hydrogen-fluorine and deuterium-fluorine lasers. To aid in understanding the effect of the fluorine wall recombination on the operation of a fluorine chemical laser, the make up and operation of such a system is examined.

Figure 1 is a schematic representation of the general class of fluorine chemical laser systems of interest. The primary flow contains the fluorine atom source to be used in the chemical reaction which will produce the excited species for lasing. This primary flow is usually the result of some earlier chemical combustion reaction such as

$$aH_2 + bF_2 + cH_e + dH + eHF + fF_2 + cHe \qquad (1)$$

where the H_2 is present in sufficient quantity to cause a large enough reaction with the fluorine to raise the temperature of the gas to a temperature level compatible with the desired nozzle input quantities of atomic fluorine, which is for the most part present from thermal dissociation of the molecular fluorine. The helium is representative of a diluent added to bring the properties of the gas to those compatible with the total laser flow system, nozzle bank, lasing cavity and diffuser section.

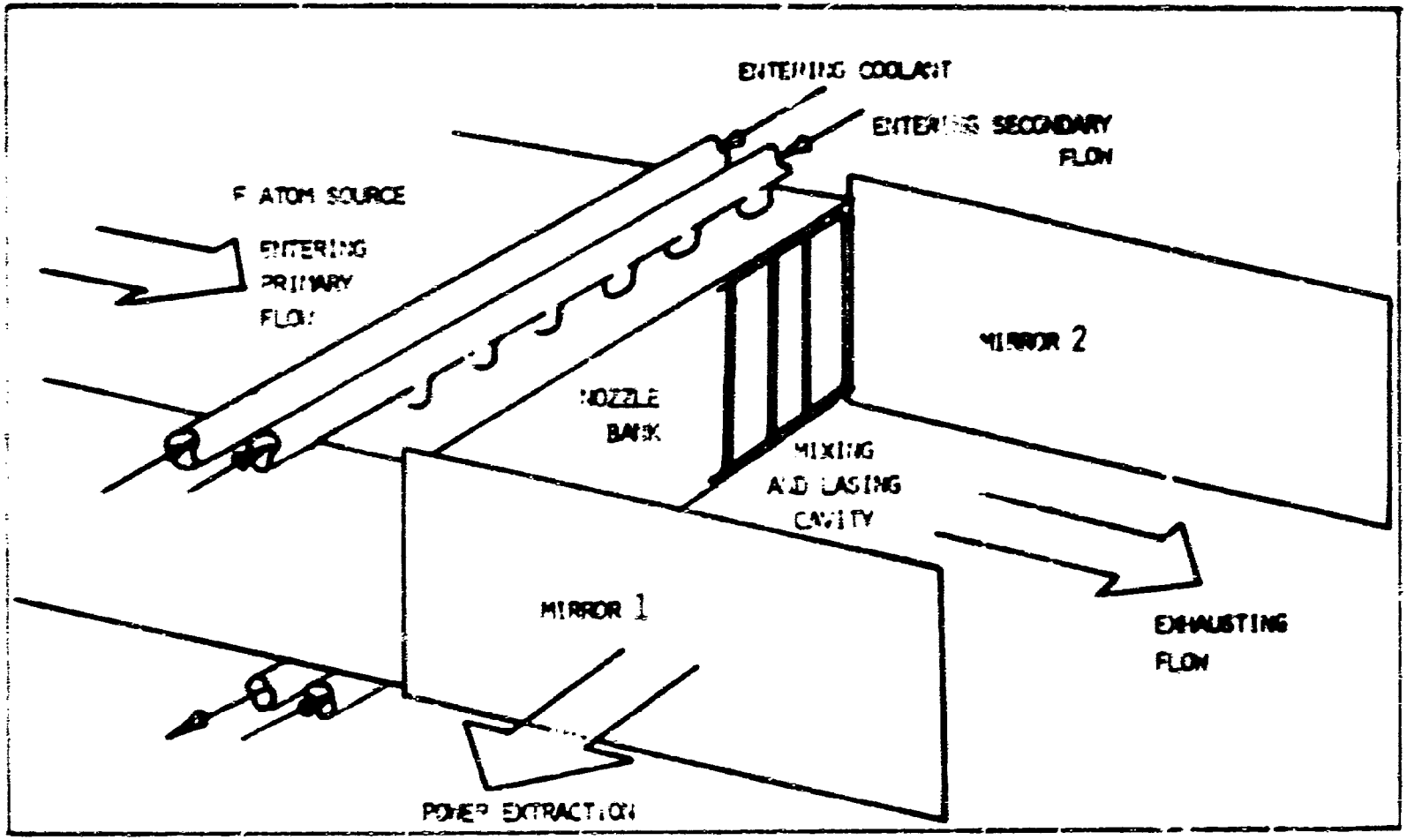

Figure 1. Chemical Laser Operation

Referring to Figure 2, the primary flow is then accelerated through the primary nozzles of the nozzle bank reaching velocities ranging from Mach 2 to Mach 5 depending on the particular laser configuration. It is on the walls of these nozzles that the fluorine recombination can take place. Upon exit from the nozzles the primary nozzle flow is joined in the mixing and lasing cavity by the adjacent secondary nozzle flows consisting of either H_2 or D_2. The jets mix in the mixing zones indicated in Figure 2 where the excited HF(v) lasing states are formed in reactions of the type

$$H_2 + F \longrightarrow HF(v) + H \qquad (2)$$

The mirrors form the optical cavity and power is extracted from the cavity through the mirror having partial transmittance.

There are many factors bearing on the matching of theoretical gain data with observed experimental gain data (Ref 3). To mention a few areas where inadequate modeling may be responsible for the mismatching the following are given:

a) Pumping reaction rates for reactions of the type

$$F + H_2 \rightarrow HF(v) + H \qquad (3)$$

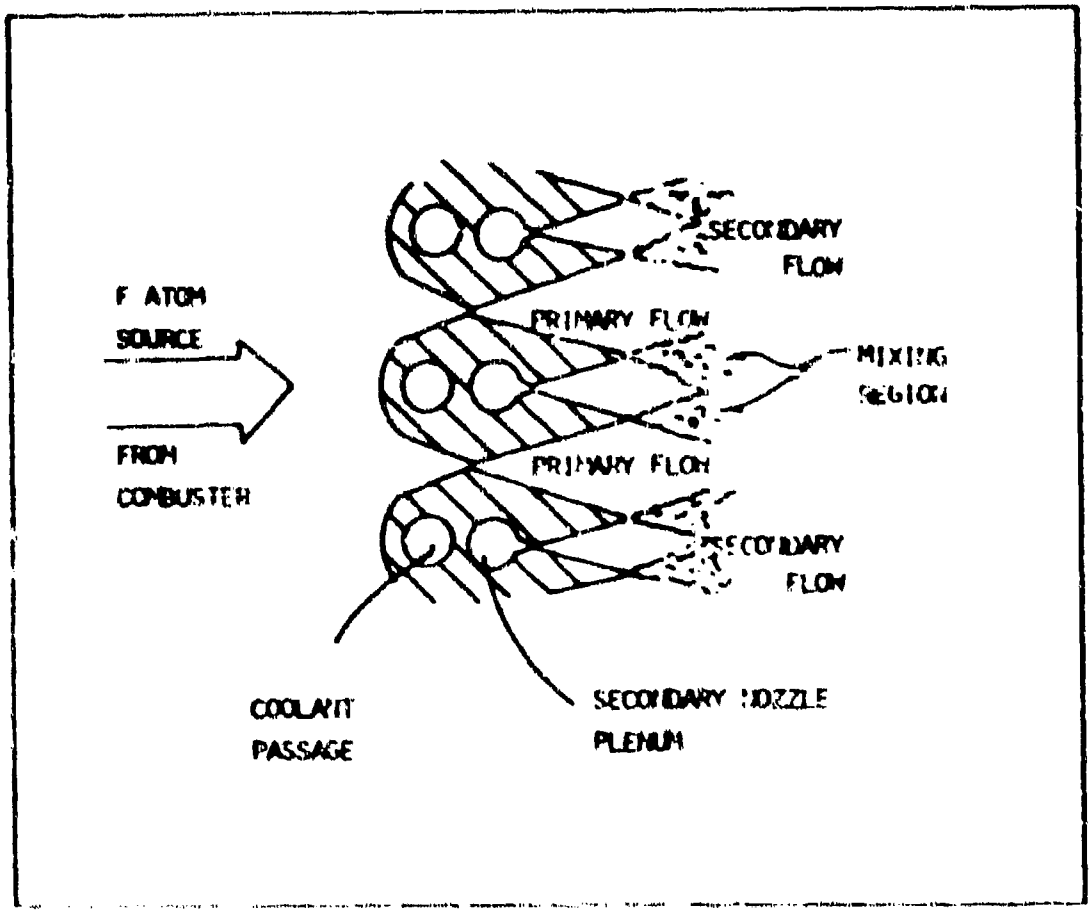

Figure 2. Cut-Away View of Nozzle Bank and Mixing Region

b) Stimulated emission relaxation rates for reactions of the type

$$HF(v) + h\nu \rightarrow HF(v-1) + 2h\nu \qquad (4)$$

c) Vibrational-rotational and vibrational-translational deactivation rates for reactions of the type

$$HF(v) + M \rightarrow HF(v-\Delta v) + M \qquad (5)$$

d) Single and multi-quantum vibrational-vibrational transfer rates for reactions of the type

$$HF(v) + HF(v') \rightarrow HF(v+\Delta v) + HF(v'-\Delta v) \qquad (6)$$

e) Turbulent mixing and diffusion processes

f) Free stream fluorine recombination rates for reactions of the type

$$2F + M \rightarrow F_2 + M \qquad (7)$$

g) Wall fluorine recombination rates

It is unclear at this time exactly how each of the factors

directly influence laser gain, as each plays an interrelated role with the others. Of particular interest in this study, however, is item g above. It is clear from Equation (2) that the wall recombination reaction is a detrimental one. The less F available to the excitation reaction, the less excited species, and thus, the less output power possible from the laser. Further understanding of the possible effect of this reaction has been pointed out by Ferrell, Kendall, and Tong (Ref 4) and Mikatarian, Kurrius, McDanal, and Thorenes (Ref 5). Ferrel et.al. showed that one might expect a large reduction in atomic fluorine and a pronounced gradient in the atomic and molecular concentration profiles at the exit plane of the primary nozzles in a study in which every fluorine atom colliding with the wall was assumed to result in a recombination. Mikatarian et.al. showed the effect one might expect from such a concentration profile on the laser output. In an attempt to explain anomalies between calculated and observed performance curves, they input a crudely estimated concentration profile into a cavity mixing and lasing code. The result was that a nonuniform initial fluorine concentration profile in the laser cavity entrance caused two important effects: reduction in the gain due to a decrease of reactants and axial shifting of the excitation reactions down stream from the exit plane of the nozzles (see Figure

3). Thus a - and understanding of this reaction is of importance in any attempt to model fluorine chemical lasers.

Heterogeneous Recombination. In general the literature contains an abundance of work dealing with the problem of recombination at a catalytic surface. For the most part the work is experimental. Various mechanisms for the wall recombination process have been proposed in an attempt to correlate the data. Of these mechanisms, three appear to be possible, two involving only surface adhered atoms proposed by Hinshelwood and one involving a reaction between a gas phase and a surface adhered atom by Rideal (Ref 6,7). These mechanisms are briefly described below:

(1) In the Hinshelwood neighboring adhered atom model it is proposed that the mechanism for recombination is the adsorption of the reactants at neighboring surface sites. Because of the necessity of neighboring collisions, this model predicts a second order reaction rate with respect to pressure at all temperatures.

(2) In the Hinshelwood migration of adhered atom model it is proposed that the mechanism for recombination is the slow adsorption of reactant specie anywhere on the surface and rapid surface migration of the adsorbed reactants followed by recombination. Since every collision which produces an adhered atom can cause a reaction, this

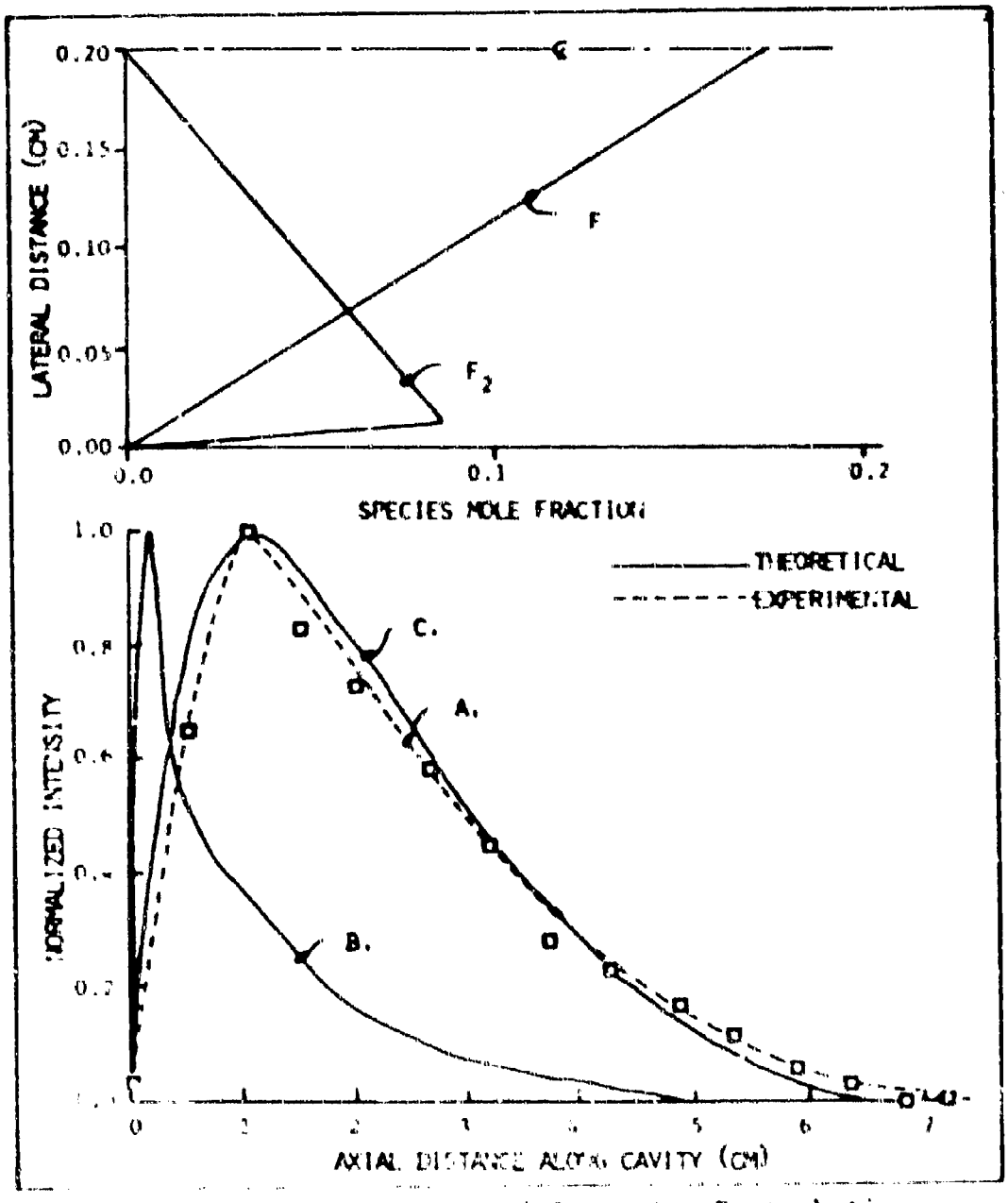

Figure 3. Calculated Normalized Intensity Distribution vs. Experimental Normalized Intensity Distribution (Calculations Made with Lockheed Laser And Mixing Program, LAMP, Ref 5)

A. Experimental Curve
B. Calculations Made with Uniform Profile of Species
C. Calculations Made with Species Profiles Shown Above

model predicts a first order reaction rate with respect to pressure at all temperatures.

(3) In the Rideal model it is proposed that the mechanism for recombination is a reaction by collision of a gas phase atom with an adhered surface atom. This mechanism, unlike the two previous ones, predicts both a first and second order reaction with respect to pressure over a range of temperature.

The currently favored mechanism is the Rideal model since the experimentally observed pressure dependence is first order at low temperatures changing to second order at higher temperatures for slow wall recombination reactions. This is the same temperature dependence predicted by the Rideal model (Ref 6,8).

With the use of the Rideal model and the assumption of an Arrhenius rate process, the various catalytic wall recombination reactions have been quantified using the experimental data for that reaction. Notably, however, a theoretical basis for explaining some experimental anomalies is very weak (Ref 9). Because of the lack of experimental data, catalytic wall recombination models for fluorine, and in fact all the Halogens, do not exist.

Review of Available Data for Halogen Wall Recombination. Very little data on Halogen surface recombination were found in the open literature. Work done by F. A. Ogryzlo

(Ref 10, 11) indicated that approximately one in ten wall collisions resulted in a recombination for chlorine and bromine atoms with a metal surface at room temperature. Ogryzlo reported that fluorine was too difficult to handle and thus no fluorine rates were measured.

W. Valance, B. Birang, and D. MacLean (Ref 12) reported that approximately one in 10^4 wall collisions resulted in a recombination for fluorine on quartz at room temperature. No work was completed by this team on interactions of fluorine with metal surfaces.

A carefully prepared set of unpublished data, however, was found to exist for fluorine recombination on a nickel surface and was made available for this study by Dr. Casper J. Ultee of United Aircraft Research Laboratories (Ref. 13).

Objectives and Scope of the Present Study

This study had three objectives: (1) Develop for the first time a quantitative model for fluorine recombination at three metal surfaces commonly used in laser nozzle construction - copper, gold, and nickel. (2) Compare the model with existing fluorine wall recombination data. (3) Use the model to examine the effect of "real" fluorine wall recombination (model verified by experimental data) on the flow in a typical chemical laser nozzle.

The development of the fluorine wall recombination model is presented in Chapter II. The approach was to adapt the Rideal mechanism as the dominant reaction mechanism (consistent with known recombination principles), decompose this mechanism into its component physical processes, and quantify each of these processes from basic principles. This differs from the conventional approach of proposing a mechanism and adjusting its bulk parameters by choosing the best fit to experimental data. By taking the basic principle approach, the model is able to take into account the detailed environment in which the reaction takes place. This leads to the inclusion of diluent effects, which have not been carefully treated in wall recombination theories for any gas.

Chapters III and IV deal with objective two, the comparison of the model with the Ultee recombination data. Chapter III develops the analytic tools necessary for this comparison and the results are presented in Chapter IV.

Chapter V deals with objective three, determining the effect of "real" fluorine wall recombination on the flow in a particular chemical laser nozzle. A description of a steady state, two-dimensional chemically reacting laminar boundary layer computer code developed for this study is included. Finally, the results of the nozzle analysis are presented.

II. Fluorine Wall Recombination Model

The Rideal mechanism was adapted as the dominant reaction mechanism because of previous verification for slow reaction regimes. The term "model" is taken here to mean the quantification of the terms in the rate equations describing the processes of the wall recombination mechanism. The model seeks to adequately describe a reactive interaction between a gas phase fluorine atom and a surface adhered fluorine atom to produce a fluorine gas molecule in an attempt to extend verification of the Rideal mechanism to reaction regimes which differ from those previously verified. Gas kinetics were examined to describe the gas phase atom behavior at the surface. The atom-wall interaction phenomenon was examined to establish the surface atom concentration. And finally, the rate equations were written and solved for the steady state case to fully establish the reaction model. A summary of each of these efforts is given in the following.

Gas Phase Kinetics

Kinetic theory was used to derive the rate of impingement of atoms on a surface and probability distribution for the normal component of the velocity of the impinging atoms. The differential flux of atoms on a surface for a Boltzmann distributed gas is given by

(Ref 14)

$$d\dot{N} = nV_3\left(\frac{m}{2\pi kT}\right)^{3/2} e^{-\frac{m}{2kT}\left(V_1^2 + V_2^2 + V_3^2\right)} dV_1 dV_2 dV_3 \qquad (8)$$

where n is the number density of atoms, V_1, V_2, and V_3 are the cartesian velocity components of the atoms, where V_3 is the normal component, m is the mass of the atom, k is the Boltzmann constant, and T is the temperature. The rate of impingement was found by integrating Equation (8) between the following limits: V_1, $-\infty \to \infty$; V_2, $-\infty \to \infty$; and V_3, $0 \to \infty$.

$$\dot{N} = n\left(\frac{kT}{2\pi m}\right)^{1/2} \qquad (9)$$

Equation (9) was used to normalize Equation (8),

$$\frac{d\dot{N}}{\dot{N}} = \frac{m^2}{2\pi k^2 T^2} V_3 e^{-\frac{m}{2kT}\left(V_1^2 + V_2^2 + V_3^2\right)} dV_1 dV_2 dV_3 \qquad (10)$$

Finally Equation (10) was integrated over all possible values of V_1 and V_2 yielding the probability density distribution of the non-dimensional normal velocity component, $\frac{V_3}{\sqrt{\frac{2kT}{m}}}$

$$P\left(\frac{V_3}{\sqrt{\frac{2kT}{m}}}\right) = \frac{2\,V_3}{\sqrt{\frac{2kT}{m}}} e^{-\left(\frac{V_3}{\sqrt{\frac{2kT}{m}}}\right)^2} \qquad (11)$$

A plot of Equation (11) is given in Figure 4.

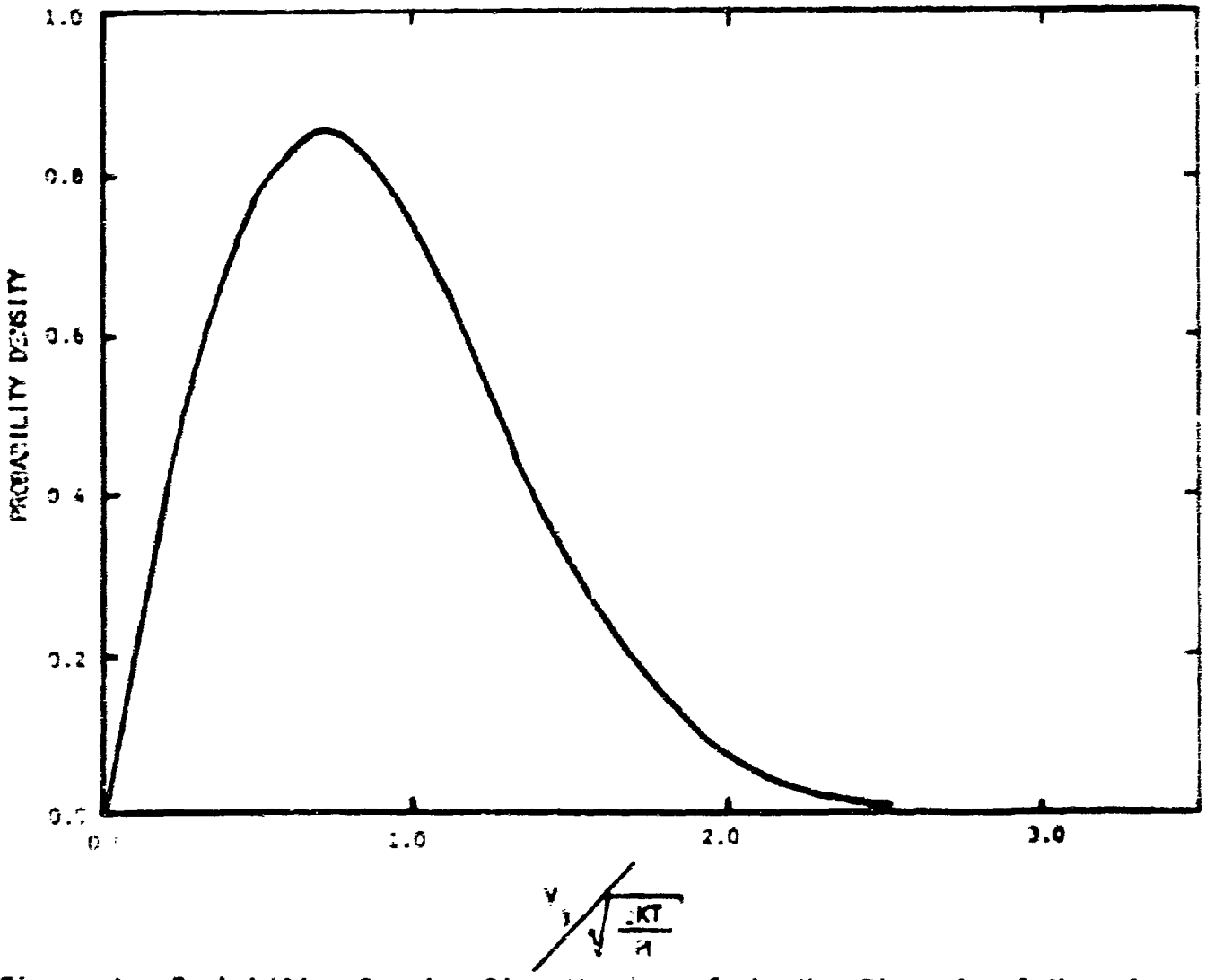

Figure 4. Probability Density Distribution of the Non-Dimensional Normal Velocity Component at a Wall

Wall Interaction Phenomena

The model required a wall adhered fluorine atom concentration. To this end the bonding potential was examined. According to Emmett (Ref 6) there are two types of wall bonding phenomena divided into two temperature regimes in which the mechanisms are predominant. These regimes are known as the low temperature regime, dominated by Van der Waal or physical bonding, and the high temperature regime dominated by chemical or activated bonding. Because of the operating temperatures of the chemical lasers of concern, this study was confined to the so called low temperature regime which limited its applicability to temperatures below approximately 800 K. Above this temperature the actual transition to chemical bonding is not known for fluorine and will not be discussed here.

Potential Well for Physical Adsorption. A simple model was constructed for the potential well near a surface based upon an adsorption (attractive) potential and a repulsive potential as suggested by Lennard-Jones (Ref 15). The model is described using copper as an example. The closest distance of approach of copper atoms in metal is 2.54 Å, while that for fluorine atoms is 1.28 Å (Ref 16). The equilibrium distance, R_E, must then be the mean of the two distances or 1.91 Å. At this equilibrium distance the repulsive forces are from 1/3 to

1/2 that due to the attractive potential. Thus by modeling the repulsive force as 40 percent that of the attractive force, a well depth was arrived at by algebraically summing the two potentials. Therefore an attractive potential, assumed to be W(r), yielded a well depth, ΔE_w, at the equilibrium position of

$$\Delta E_w(R_E) = 0.6\ W(R_E) \qquad (12)$$

No reference is made to an activation energy and in fact no activation energy is experimentally observed for physical adsorption (Ref 6). The potential well is shown in Figure 5.

Several authors have described the functional relationship of W(r). The earliest of these descriptions (Ref 15) was the simplest and yielded fair results. As reported by several authors (Ref 17,18, and 19), this early model served as an upper limit on the physical attractive force that one might expect to find. One of the more recent papers dealing with the subject was that of C. Mavroyannis (Ref 20). In his paper, Mavroyannis derived a formula for W(r) and compared the results of his relationship with four previously derived relationships, those of Lennard-Jones, Bardeen, Margenau and Pollard, Prosen and Sachs (Ref 15,17,18, and 19). The results of

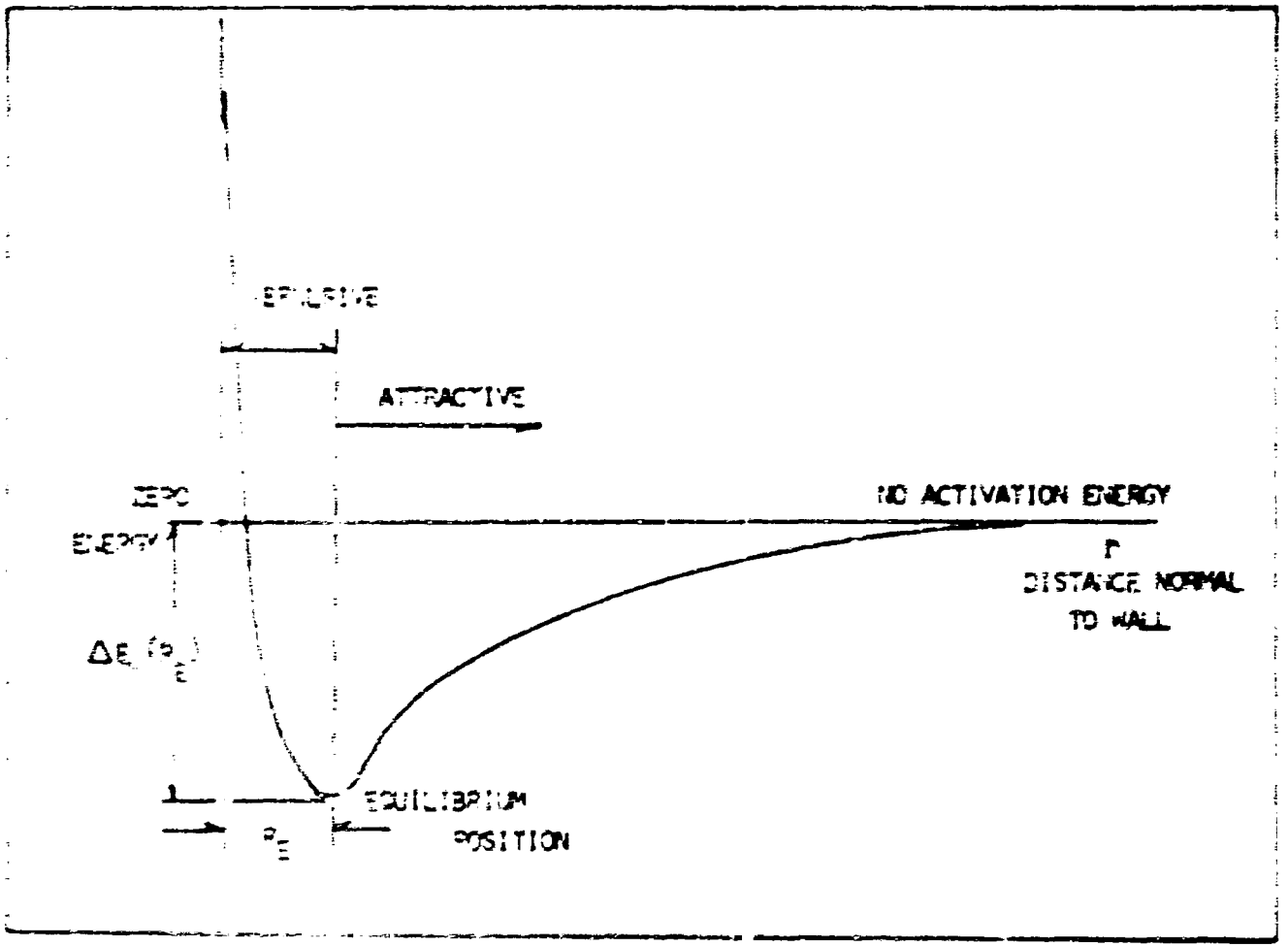

Figure 5. Physical Adsorption Potential Well

his comparison showed that his model compared as well as, and in most cases better than the previous models with data for several atom-surface systems. In addition, the Mavroyannis model made use of readily available material properties. For these reasons the Mavroyannis potential was adopted for use in the fluorine recombination model. The formula for this potential is given below

$$W(r) = - \frac{\langle q^2 \rangle}{12r^3} \frac{\frac{\hbar W_p}{2^{1/2}}}{\frac{3}{2}\frac{N}{\langle q^2 \rangle} + \frac{\hbar W_p}{2^{1/2}}} \qquad (13)$$

where r is the distance of separation as in Equation (12), $\langle q^2 \rangle$ is the sum of the electronic charge of each electron in the adhered atom times the expectation value of its orbital radius squared, $\hbar W_p$ is the work function of the metal surface and N is the number of electrons in the adhered atom.

The Interaction Between the Gas Phase Atom and the Wall in the Presence of an Adsorption Potential. Given the functional form of the Mavroyannis adsorption potential and the Lennard-Jones functional relationship for the potential well depth, the well depth was used to determine the probability of an atom of some given energy adhering to the wall. Out of several possible methods of addressing the atom-surface collision process in the presence of a wall potential reported on the literature, the soft cube

model presented by Logan and Keck was chosen (Ref 21). Some results of this model were recently presented by Pagni and Keck (Ref 22) and Modak and Pagni (Ref 23).

The Soft Cube Model. As dictated by the soft cube model, the surface of the wall was pictured as made up of wall atoms vibrating at a frequency consistent with the bulk Debye temperature in a direction normal to the plane of the surface. The overall picture was that of an infinite checkerboard with each square made up of one atom vibrating randomly into and out of the surface at the Debye frequency, w_s. During a surface interaction only the velocity component of the gas phase atom normal to the surface was considered. The use of the normal velocity component enabled data correlation which was not able to be made using the total velocity in the case of low incident angle atom-surface collisions. The gas phase atom was further assumed to interact with only one surface atom. The various frequencies and potentials were then modeled as shown in Figure 6. The shape of the well beyond the interaction position was of no importance. The gas atom was simply given additional velocity above its Boltzmann predicted gas phase velocity consistent with the well depth. As discussed by Modak and Pagni the interaction spring constant, k_g was modeled by an exponential repulsive potential, V(r),

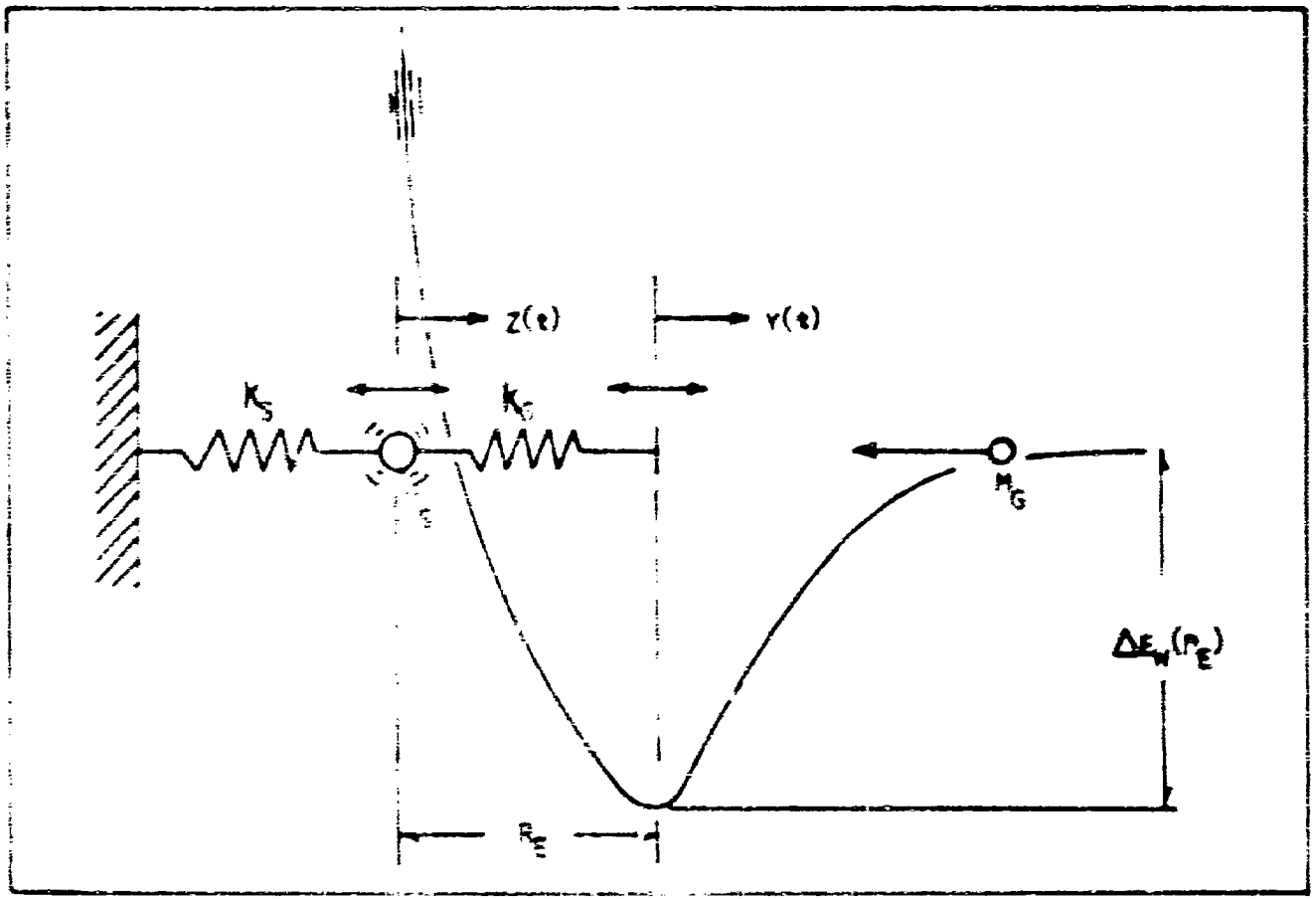

Figure 6. Gas-Wall Collision Model

$$V(r) = C \left\{ \Delta E_W(R_E) \right\} e^{-\frac{r}{\alpha}} \tag{14}$$

where r is the position, α is the distance over which the interaction took place, and C and B are constants adjusted to match experimental data. The spring constant was obtained from Equation (14) by differentiation to obtain the force, and expansion of this force around r = 0 keeping only up to the linear term. Matching the boundary condition that the force = 0 at r = 0 yielded a spring constant, k_g,

$$k_g = \frac{.2\ D^{1.17}}{\alpha^2} \tag{15}$$

where D is the well depth. The spring constant for the surface atom was given by

$$k_s = \omega_s^2\ m_s \tag{16}$$

A collision began when a gas phase atom, m_g, came in contact with the moving end of the spring k_g. From this point until the collision ended the system acted as a simple undamped two mass system. A collision then took place with a gas phase atom of velocity v

$$v = V_3 + \sqrt{\frac{2\Delta E_w(R_E)}{m_g}} \tag{17}$$

where V_3 is the Boltzmann predicted random surface normal component of velocity (see Equation (11)). The Y(0) position of the spring at collision was also random but equal to Z(0) The initial conditions were

$$Z(0) = Y(0) \tag{18}$$

$$v > \dot{Y}(0) \tag{19}$$

Equation (19) is interpreted to mean that if the velocity v were less than $\dot{Y}(0)$ there would have been no collision.

The collision ended at t_c when $Y(t_c) = Z(t_c)$. At that point, if $1/2\ m_g(v(t_c))^2 < F_w(R_E)$ the atom was trapped and if $1/2\ m_g(v(t_c))^2 \geq F_w(R_E)$, the atom escaped the well and avoided trapping.

Referring to Figure 6, the equations of motion for the collision process are given by

$$\begin{aligned} m_g\ddot{Z} + (k_g + k_s)Z - k_gY &= 0 \\ m_g\ddot{Y} - k_gZ + k_gY &= 0 \end{aligned} \tag{20}$$

The detailed solution of Equations (20) is given in Appendix A. The results of this solution yielded the functions $\hat{Y}(t)$, $\hat{Z}(t)$ and $Y(t)$. Using the collision criteria above, stick or no stick decisions were made for given sets of initial conditions.

Rate Process and Equations

The stick or no stick decisions, as described in Appendix A, required 40 calculations for each of 26 initial non-dimensional velocity conditions predicted by a Boltzmann distributed gas for a given temperature. Twenty temperatures were run between 0 K and 800 K for each gas-metal system. The result of this process yielded an initial or clean surface sticking coefficient, $S_o(T)$, defined as the statistical probability that any given collision of a gas phase atom with the surface at temperature T would result in the atom being trapped by the surface. The actual sticking coefficient as a function of surface coverage, θ ($\theta = 1$ being a fully covered monolayer of adhered surface atoms), was experimentally verified by Christmann et.al. (Ref 24) to be

$$S(T,\theta) = (1-\theta)S_o(T) \qquad (21)$$

The sticking coefficient was then used in describing the rate equation for the time rate of change of the

surface adhered atom concentration by

$$\frac{d(n_s)_F}{dt} = S_o(1 - \theta)\dot{N}_F - \delta_F\theta - S_t\dot{N}_F\theta \qquad (22)$$

where n_s is the surface concentration and $\dot{N}_F$ is the rate of impingement of F atoms as described earlier. The depletion of the surface concentration described by the last two terms of Equation (22) was given by the thermal desorption rate, δ, times a surface coverage θ (Ref 6) and the detachment caused by recombinations was represented by a steric factor S_t, the surface coverage θ, and $\dot{N}_F$. The thermal desorption rate used was that given by Glasstone, Laidler and Eyring (Ref 25)

$$\delta = C_a \frac{kT}{h} e^{-\frac{E_D}{RT}} \qquad (23)$$

where C_a was the number of surface sites per unit area (metal surface atom packing), h the Planck constant, and E_D a desorption energy. The packing used was that of the face centered cubic for all surfaces considered (Ref 26). The steric factor S_t is the ratio of the gas phase-surface adhered atom collisions resulting in a recombination to the actual number of these collisions.

The surface coverage of interest in Equation (22) was of course that of the fluorine atoms. Since the actual

number of adhered atoms depended on the number of available surface sites, the presence of adhered atoms other than fluorine effectively decreased the surface area available for fluorine to adhere. In this light, Equation (22) was rewritten as follows

$$\frac{d(n_s)_F}{dt} = (S_o)_F \hat{N}_F (1 - \theta_T) - \delta_F \theta_F - S_t \hat{N}_F \theta_F \qquad (24)$$

where θ_F represented the fluorine surface coverage and θ_T represented the total surface coverage which included other as well as fluorine atoms.

To quantify θ_T a rate equation was written to include the effect of any diluent which might have been present. This rate equation was given by

$$\frac{d(n_s)_D}{dt} = (S_o)_D \hat{N}_D (1 - \theta_T) - \delta_D \theta_D \qquad (25)$$

where Equation (25) reflects only one subtracting term, that of thermal desorption. For one diluent then, $\theta_T = \theta_F + \theta_D$, assuming molecular species do not adhere.

Solving Equation (24) and (25) for the steady state condition yielded

$$\theta_D = \frac{1}{1 + \frac{\delta_D}{(S_o)_D \hat{N}_D}} (1 - \theta_F) \qquad (26)$$

$$\theta_F = \frac{1}{1 + \frac{\delta_F}{(S_o)_F \dot{N}_F} + \frac{S_t}{(S_o)_F}} (1 - \theta_D) \qquad (27)$$

Further, solving Equations (26) and (27) simultaneously

$$\theta_F = (\theta_F)_o \left| \frac{1 - (\theta_D)_o}{1 - (\theta_F)_o (\theta_D)_o} \right| \qquad (28)$$

where

$$(\theta_F)_o = \frac{1}{1 + \frac{\delta_F}{(S_o)_F \dot{N}_F} + \frac{S_t}{(S_o)_F}} \qquad (29)$$

$$(\theta_D)_o = \frac{1}{1 + \frac{\delta_D}{(S_o)_D \dot{N}_D}} \qquad (30)$$

$(\theta_F)_o$ and $(\theta_D)_o$ were defined to correspond to the actual coverages of one in the absence of the other.

Having solved for the surface coverage of atomic fluorine, the recombination rate, v_R, was given simply by

$$v_R = S_t \dot{N}_F \theta_F \qquad (31)$$

Finally the recombination coefficient, γ, defined as the ratio of fluorine atom wall collisions resulting in a recombination to the total number of fluorine atom wall

collisions, was given by

$$\gamma = \frac{v_R}{\dot{N}} = S_t \theta_F \tag{32}$$

III. Low Pressure Pipe Flow with Wall Recombination

A simple model of one-dimensional volumetric fluorine depletion applicable in low pressure pipe flow was developed to simulate the Ultee experiment (Ref 13).

Ultee Experiment

The Ultee data were taken in the experimental apparatus described pictorially in Figure 7. Gas of known F_2 concentration and a diluent (argon) flowed from the gas source into a microwave discharge cavity where the molecular fluorine was dissociated to atomic fluorine. Measurements taken at the exit of the cavity without the test sample tube attached showed that approximately 10 percent of the F_2 was dissociated. This fixed the gas mixture of F, F_2 and Ar at the entrance of a 75 cm X 1.1 cm (I. D.) test sample tube made of various catalytic metals. Of interest here was the nickel sample. The pressure drop across the sample, the equilibrium temperature of the sample and the flow rate of the gas were monitored and recorded. An ESR spectrometer located at the end of the test sample yielded information from which F and F_2 concentrations were calculated. The gas then left the test apparatus through the pumping system. For each data point the system was allowed to come to equilibrium at the particular

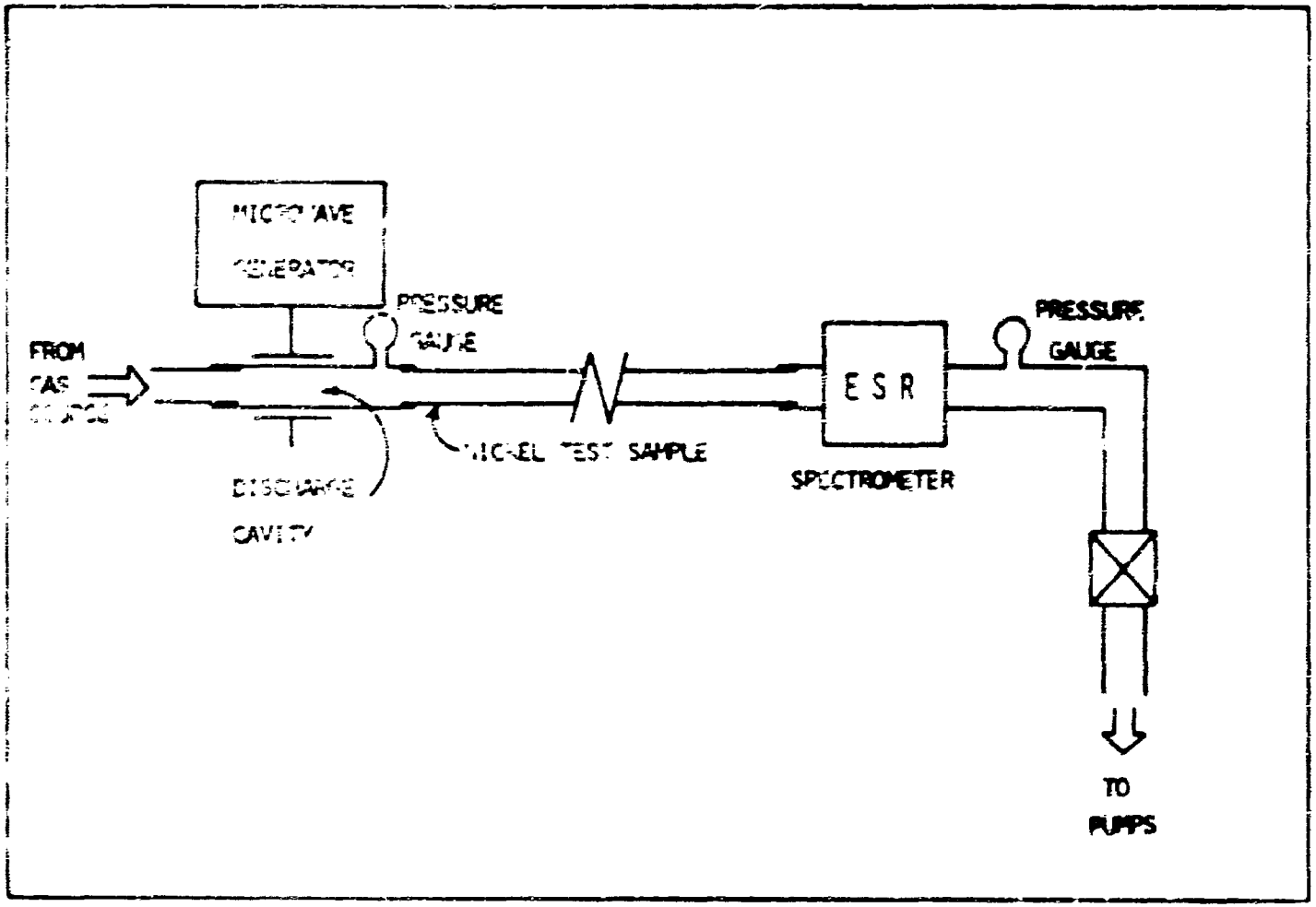

Figure 7. Ultee Experimental Apparatus

temperature of interest, always keeping a constant initial pressure and flow rate throughout the experimental range of temperatures.

Analytic Model

Under the assumption of a one-dimensional dependence of the concentration on axial position in the test sample, the equation of the process was written as follows (see Figure 8)

$$\frac{dn}{dx} = -\frac{4\gamma n}{Ur}\left(\frac{kT}{2\pi m}\right)^{1/2} \tag{33}$$

where n is the number density, x the axial position, r the tube radius, γ the recombination coefficient, U the flow velocity, and $n\,(kT/2\pi m)^{1/2}$ the rate of impingement. Equation (33) has an analytic solution under the assumptions of a constant recombination coefficient γ and an initial number density n_o

$$\frac{n}{n_o} = e^{-\frac{4\gamma x}{rU}\left(\frac{kT}{2\pi m}\right)^{1/2}} \tag{34}$$

Equation (34) can be used to determine an overall effective recombination coefficient.

Since the recombination coefficient, as described in Section II, depended on various parameters which changed with position along the test sample, more accurate

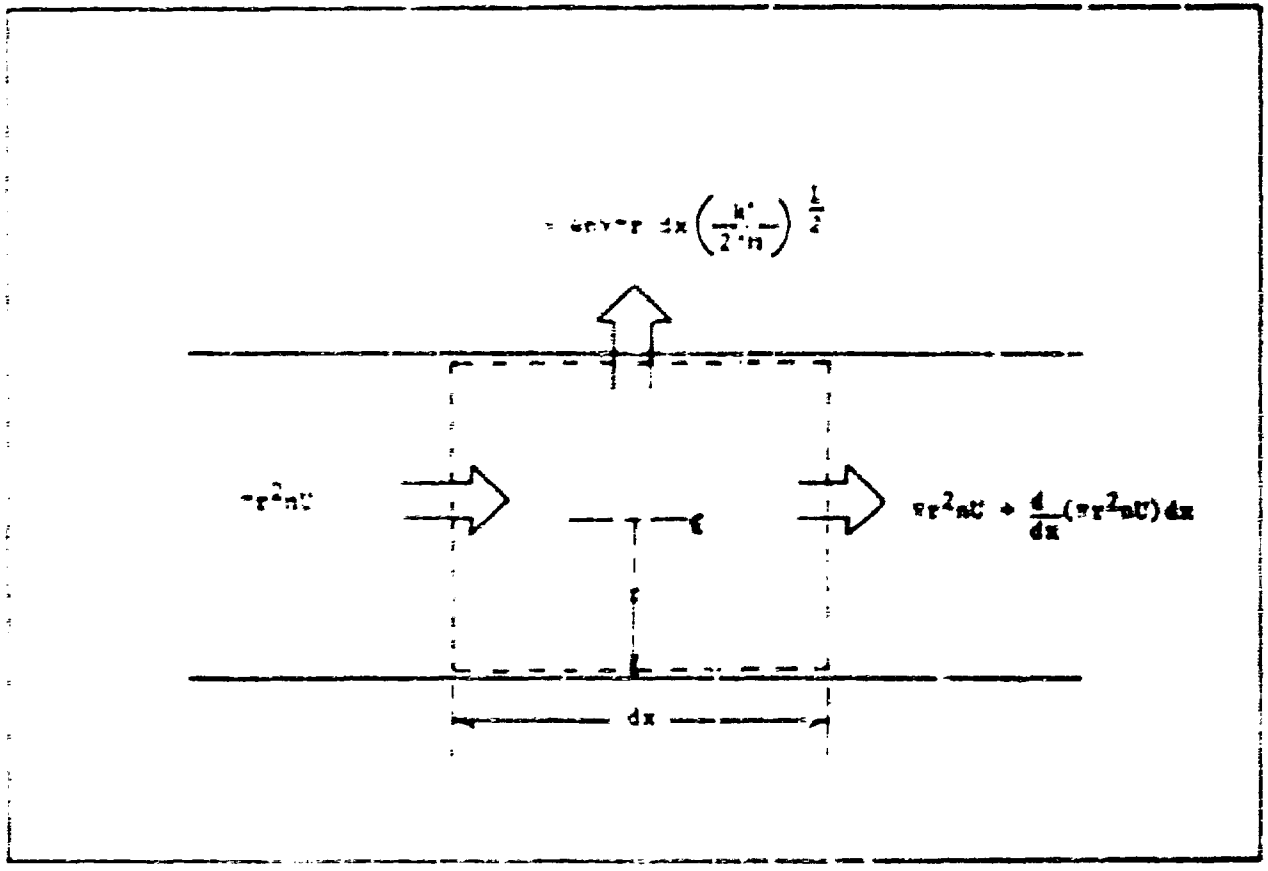

Figure 8. One-Dimensional Pipe Flow Concentration Depletion

simulation of the actual experiment was made by a step by step solution of Equation (34) for an axial grid spacing of Δx.

$$\frac{n(x_i + \Delta x)}{n(x_i)} = e^{-\frac{4\gamma(x_i)\Delta x}{rU}\left(\frac{kT}{2\pi m}\right)^{1/2}} \tag{35}$$

where the values of $\gamma(x)$ and $n(x)$ were calculated at each station to predict the change in the number density to the next station.

Applicability Criteria

As a measure of the applicability of the sole assumed dependence of the fluorine concentration on axial position, the characteristic times for diffusion and depletion can be compared. A typical time for diffusion to negate gradients can be represented by the relaxation time for diffusive equilibrium in an enclosure of dimensions r (Ref 27)

$$t_{DIFF} = \frac{r^2}{\mathcal{D}} \simeq \frac{3r^2}{\lambda \bar{v}} \tag{36}$$

where $\mathcal{D}$ is the diffusivity, λ is the mean free path and $\bar{v}$ is the average molecular velocity. This time can be compared to the time necessary for destruction of all the atoms in the volume V by recombination at the wall neglecting the effects of diffusion. The depletion time is given by

$$t_{REC} = \frac{nV}{2n\frac{\bar{v}_Y}{4} S} = \frac{r}{\bar{v}_Y} \tag{37}$$

where S is the wetted surface. For validity of the one-dimensional assumption of the concentration

$$t_{REC} >> t_{DIFF} \tag{38}$$

IV. Comparison of Theoretical Model with Experimental Data

Sticking Coefficients

The solution of the equations of motion for the collision process were integrated over the Boltzmann distribution given in Figure 4 to obtain the sticking coefficient, S_o, for fluorine, argon, and helium for three surfaces representative of fluorine laser nozzle materials; gold, nickel and copper. The results are given in Figures 9, 10, and 11. Comparison of the figures in light of the effect of diluents on recombination rates (Equations (28) through (31)) as discussed earlier indicated that argon, when used as a diluent, should have an appreciable effect on the recombination rate of fluorine, while the helium probably would not. Further mention of the helium diluent system is made later.

Ultee (Ref 13) reported that a slightly higher recombination rate may have occurred on copper than on nickel. Examination of Figure 9 shows that this is consistent with a slightly higher sticking coefficient of the fluorine on copper.

Comparison of Pipe Flow Calculations with Data

The physical parameters of the Ultee experiment are given in Table I and the computational parameters are given in Table II. Using the applicability criterion from Equation (38) it was found that calculations based on the

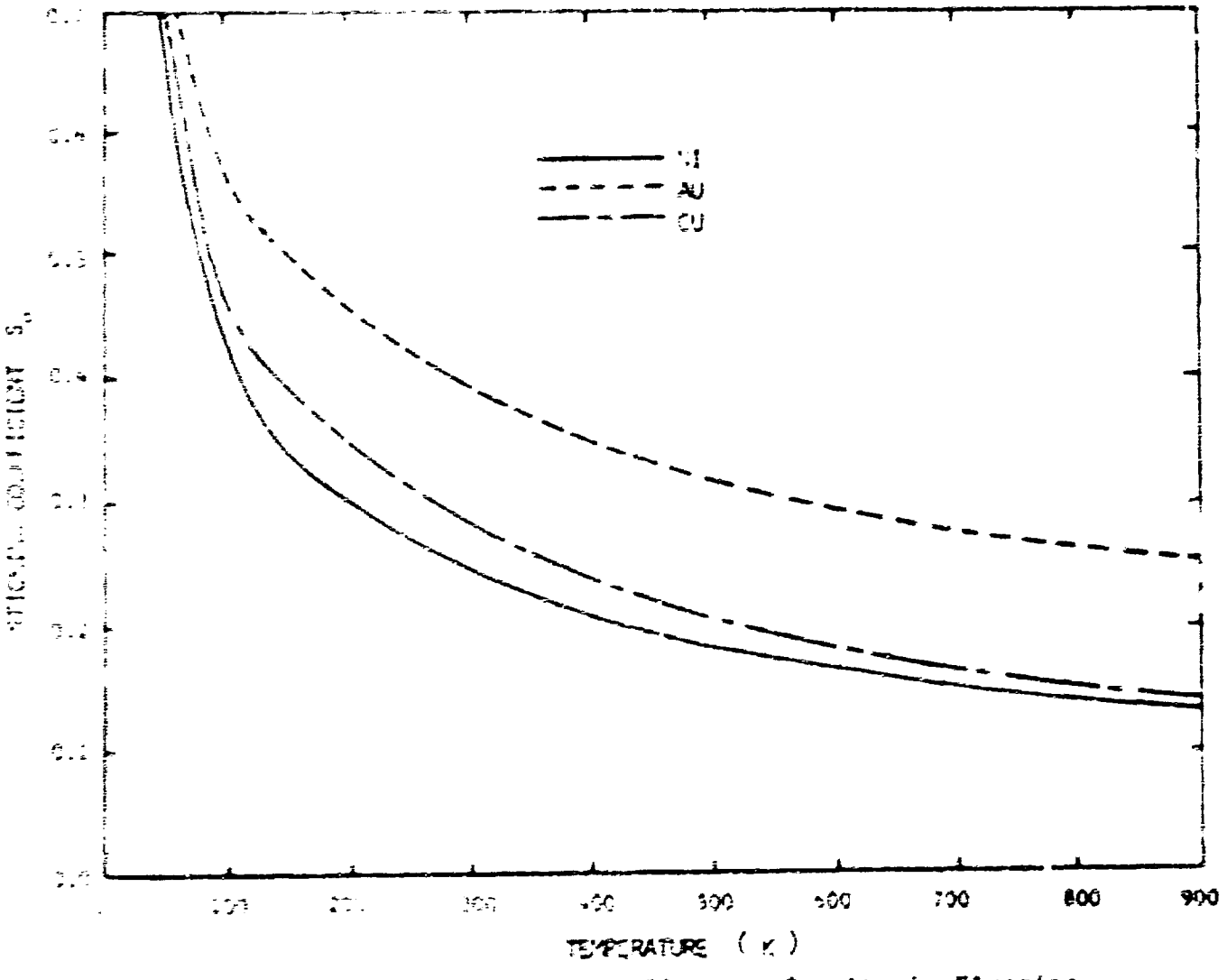

Figure 9. Sticking Coefficient for Atomic Fluorine

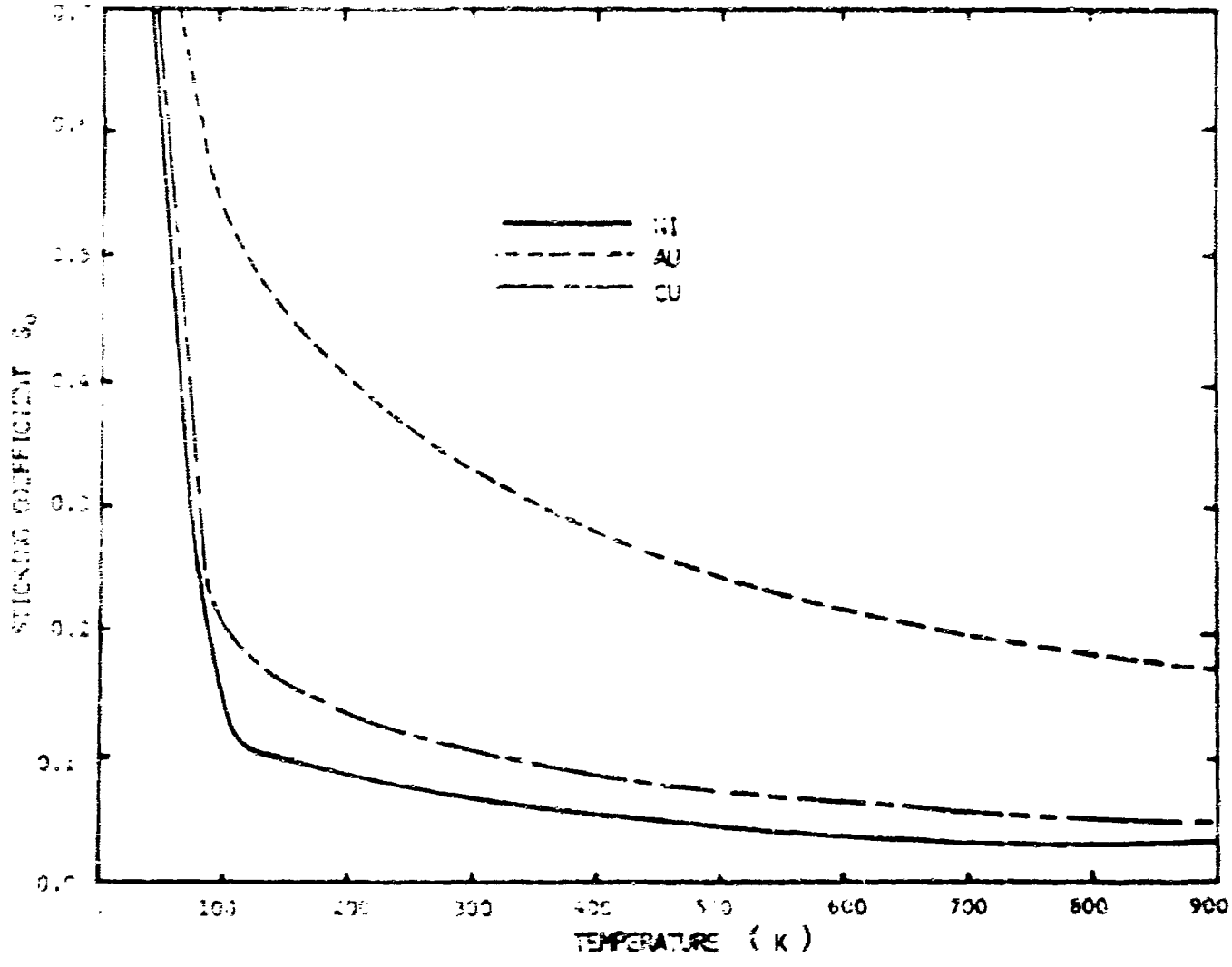

Figure 10. Sticking Coefficient for Argon

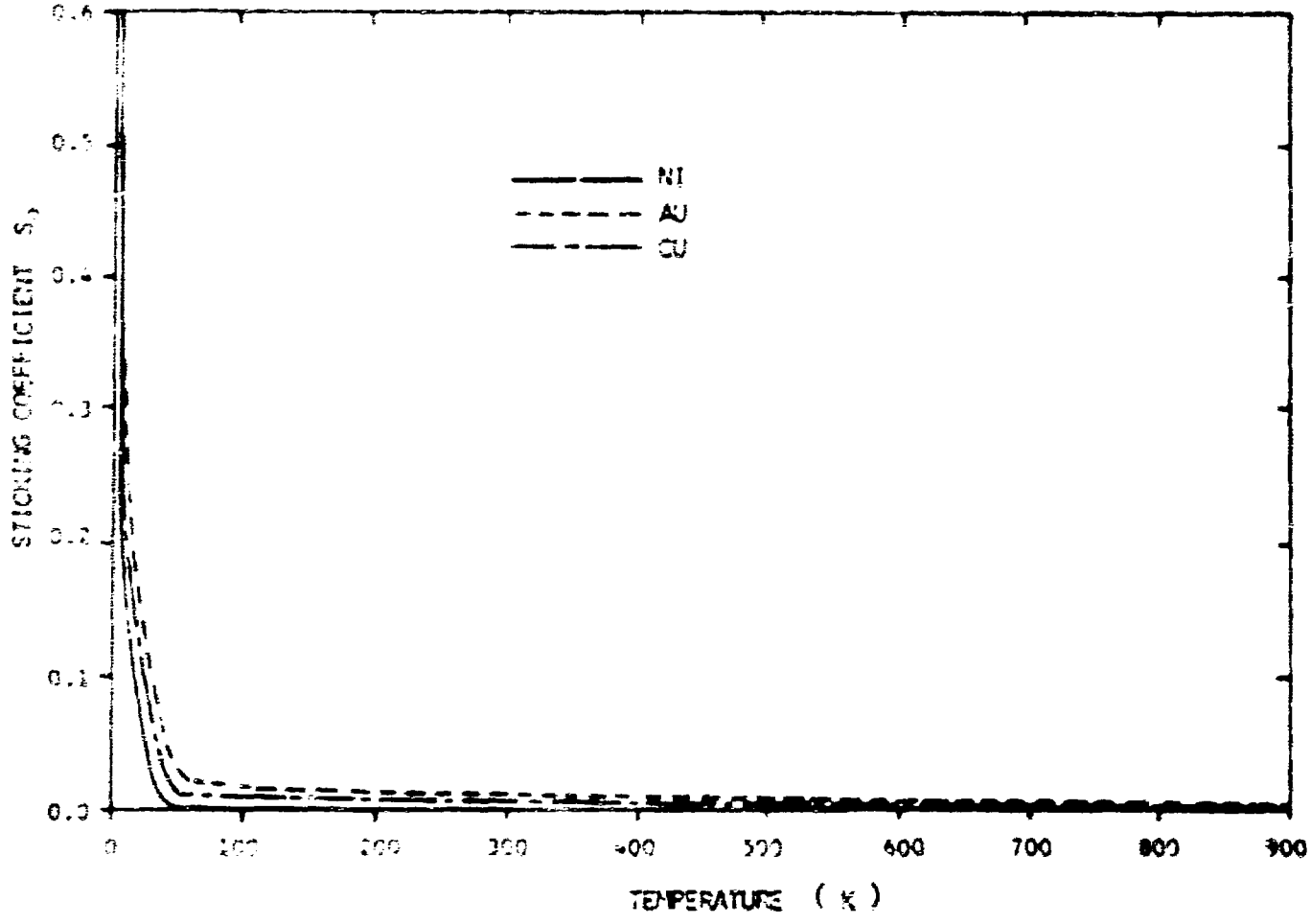

Figure 11. Sticking Coefficient for Helium

one-dimensional assumption for the test conditions of the Ultee experiment were applicable for a recombination coefficient as high as 10^{-3}. Thus the one-dimensional assumption was good for all available data points as will be shown.

Table I. Physical Parameters of Ultee Experiment

PARAMETER	VALUE
PRESSURE	2.7 TORR
FLOW VELOCITY	180 cm/sec
MOLE FRACTION AT SAMPLE ENTRANCE	
[F]	0.01
[F_2]	0.09
[Ar]	0.90
TEMPERATURE RANGE	0 °C to 400 °C
SAMPLE MATERIAL	NICKEL
SAMPLE I.D.	1.1 cm

Computations based on Equations (32) and (35) were performed for comparison with the Ultee experimental data. The results of these computations are presented in Figure 12. Shown in Figure 12 is the percent F remaining at the end of the nickel sample tube over a range of steady state temperatures. The only parameters which were arbitrarily chosen in order to have the model match the data were the desorption energies $(E_D)_F$ and $(E_D)_{Ar}$, and the steric factor

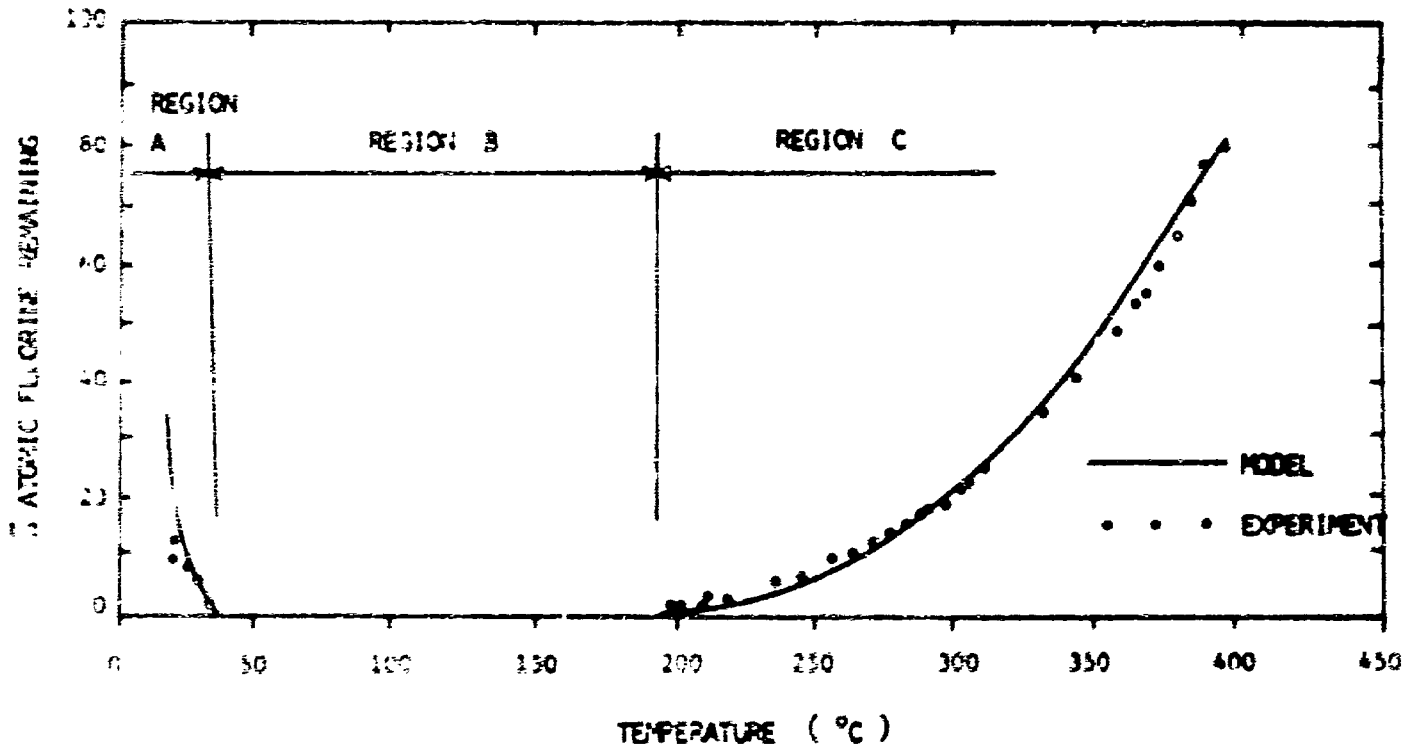

Figure 12. Comparison of Model with Experimental Data, Plotted is the % F Remaining at the End of the Nickel Test Sample vs. Steady State Temperature of the Sample.

S_t (see Table II). The desorption energies required to match the data were found to be similar in magnitude to those for other gas-surface systems reported by Emmett (Ref 6). Further, the choice of the desorption energies was rather clear since a higher or lower energy caused the curve intersection with the temperature axis to shift to the right or left, respectively. Also as an additional indicator of the correct choice of desorption energy, a higher or lower energy caused a shallower or steeper slope, respectively, although this effect was not as pronounced as the intersection shifting. The effect of varying the steric factor, S_t, is shown in Figure 13. A steric factor of 0.1 seemed to best fit the data.

Table II. Computational Parameters

PARAMETER	VALUE
m_{Ar}	6.63258×10^{-23} g
m_I	3.15431×10^{-23} g
$C_a \frac{kT}{h}$	3.3878×10^{25}
$(I_0)_I$	1.242×10^{-12} erg
$(I_0)_{Ar}$	1.173×10^{-12} erg
S_t	0.1
$(S_o)_I$	Figure 9.
$(S_o)_{Ar}$	Figure 10.

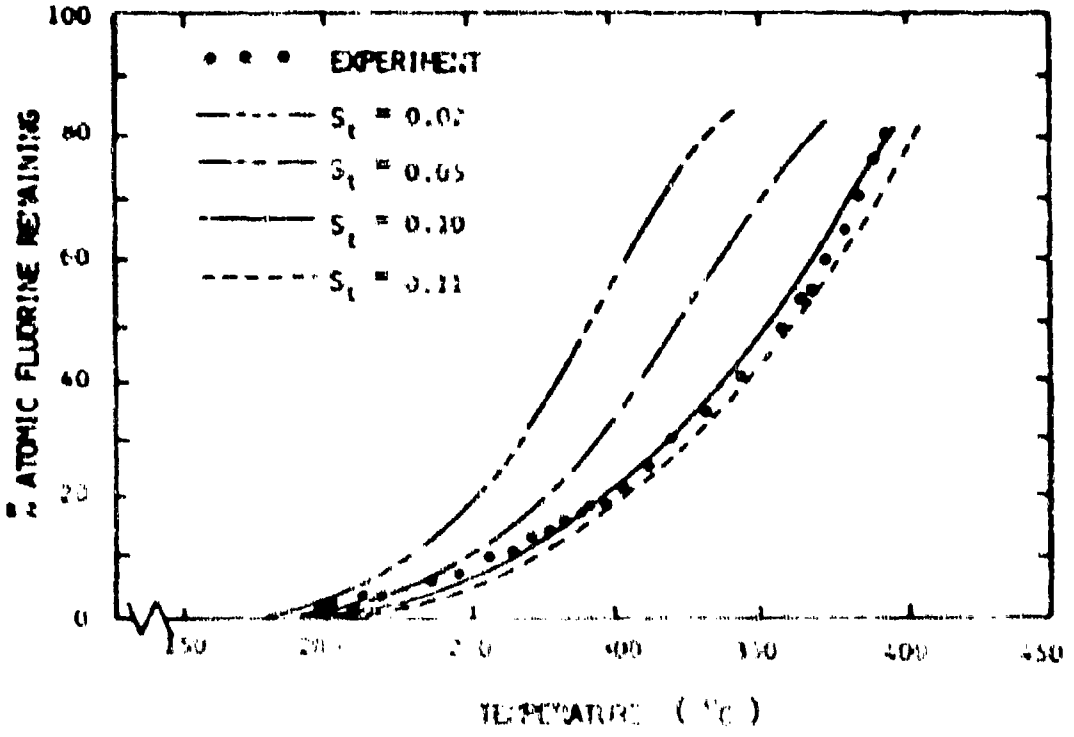

Figure 13. Effect of Varying the Steric Factor

By using the model, regions of the data were interpreted and labeled as shown in Figure 12. Region A (0 °C to 40 °C) is that region in which the wall reaction was dominated by the presence of adhered argon atoms "poisoning" the recombination process by not allowing free surface sites for the fluorine to attach. By use of Equation (30) it can be seen that prior to reaching some activation temperature for thermal desorption (i.e., $\delta_D << (S_o)_D N_D$), the argon completely covered the surface therefore rendering θ_F equal to zero. As the temperature rose the thermal desorption became important and the argon began to allow portions of the surface to be left vacant so that the fluorine could attach and subsequently recombine.

In region B, (40 °C to 195 °C) δ_F was insignificant as compared to $(S_o)_F N_F$ thus the surface coverage was determined primarily by S_t and $(S_o)_F$ so that Equation (29) could be approximated by

$$\theta_F = \frac{1}{1 + \frac{S_t}{(S_o)_F}} \tag{39}$$

Finally in region C (195 °C to 400 °C) the desorption of fluorine was activated and eventually dominated the wall reaction.

At this point it is of interest to mention Figure 14. Equation (34) was used in conjunction with the Ultec data

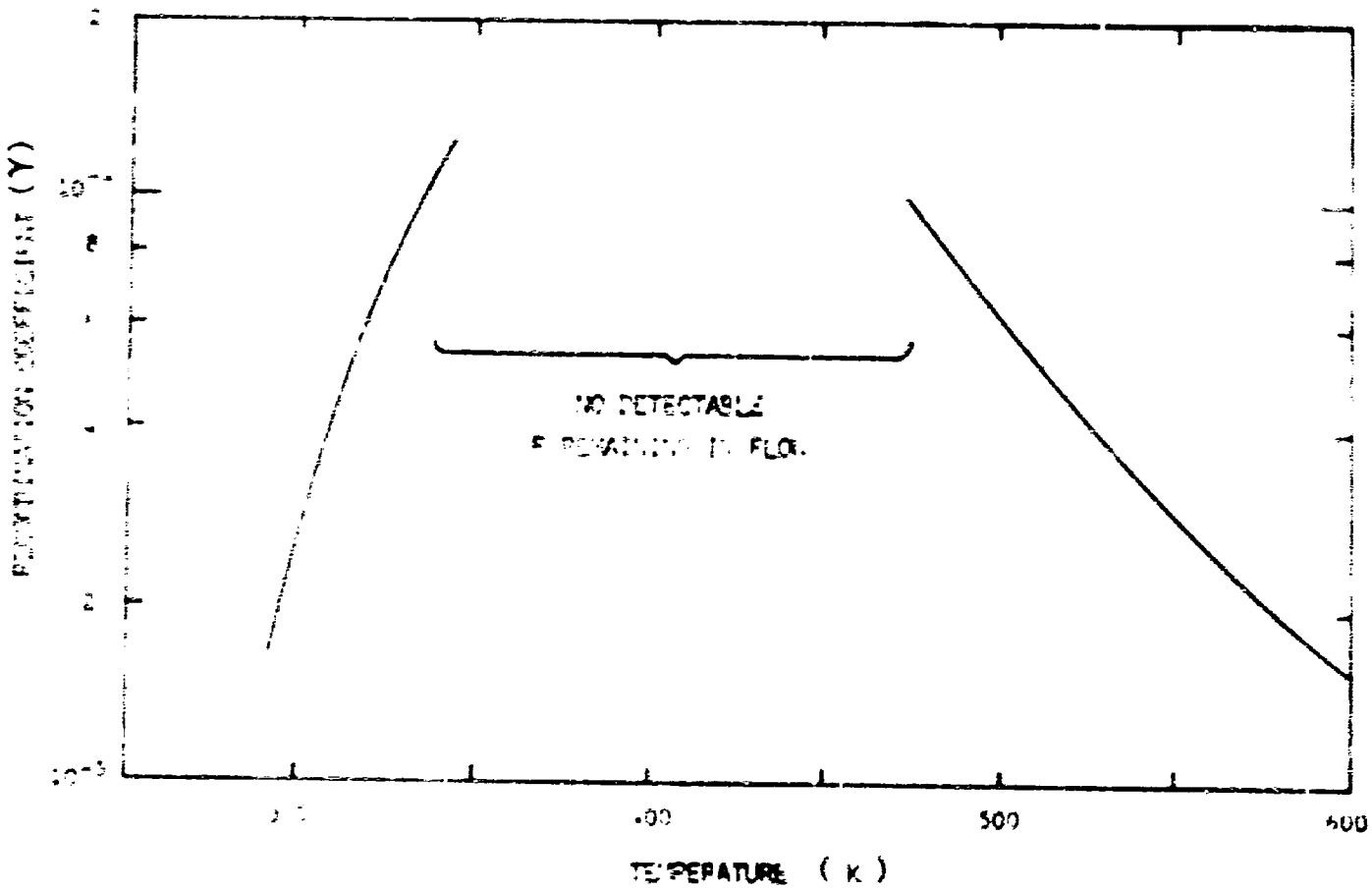

Figure 14. Effective Recombination Coefficient Calculated from Ultee Experimental Data Using Equation (34)

to obtain an average wall recombination coefficient. The result of this computation is given in Figure 14. The unknown region refers to the temperatures at which no F was detected at the exit of the test sample. Thus, at an average γ of approximately 10^{-4} all the detectable F had been removed from the flow by wall recombination. This seems to indicate that within the range of the experimental data the assumption of one-dimensional depletion was applicable. Equations (26) through (30), however, show the dependence of γ on the local number density in the $\dot{N}_F$ terms. The maximum recombination took place at the entrance of the test sample where n_F was a maximum. Figure 15 shows the temperature dependence of γ based on the maximum number density. Using the maximum γ criteria the experimental data range still falls within the one-dimensional assumption. More important, however, is the capability of determining the actual temperature and number density dependence of γ using the model. Without the model the best one could do is to determine an average γ from Figure 14 extrapolated to a maximum. Clearly the actual maximum is nearly two orders of magnitude higher than would be estimated without the use of the model. This mistaken maximum is in fact what was reported by Oltec (Ref 13). A set of maximum recombination coefficient curves for several gas pressures for 90 percent dissociated fluorine is given in Appendix D. While the

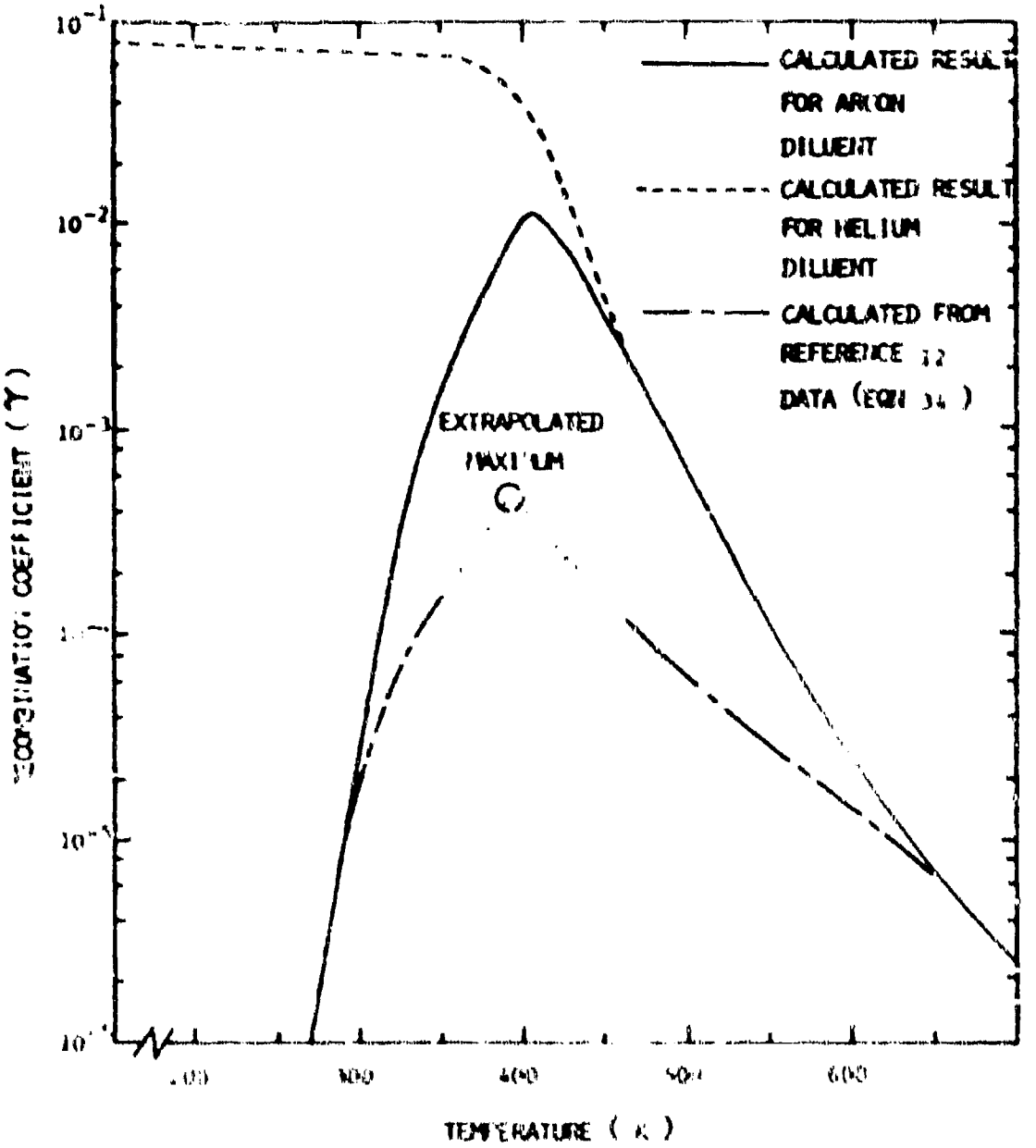

Figure 15. Maximum Fluorine Wall Recombination Coefficient vs. Temperature for a Total Pressure of 2.7 Torr, 90% Argon Diluent Flow, and 10% Fluorine Dissociation

curves for 90 percent dissociation are different than would be predicted by 10 percent dissociation the characteristic trend for increased total and partial pressures is the same.

Based upon Figure 11, it is predicted that in a similar test run with a helium diluent region A would either be nonexistent or greatly reduced from that in Figure 12, while regions B and C would show no change. The maximum recombination coefficient with a helium diluent should roughly correspond to the curve in Figure 15 represented by the dashed line.

V. Effects of Recombination in Chemical Laser Nozzles

Flow Equations

A two dimensional, steady state, laminar, explicit boundary layer code was constructed to approximate nozzle flow. The code was constructed for the purpose of demonstrating the applicability of the well recombination model to real flow systems. The governing equations are as follows under the usual boundary layer assumptions:

CONTINUITY:

$$\frac{\partial}{\partial x}(\rho u) + \frac{\partial}{\partial y}(\rho v) = 0 \tag{40}$$

MOMENTUM:

$$\rho u\frac{\partial u}{\partial x} + \rho v\frac{\partial u}{\partial y} = -\frac{dP}{dx} + \frac{\partial}{\partial y}(\mu\frac{\partial u}{\partial y}) \tag{41}$$

SPECIES:

$$\rho u\frac{\partial F_j}{\partial x} + \rho v\frac{\partial F_j}{\partial y} = -\dot{w}_j + \frac{\partial}{\partial y}\left(\rho\mathcal{D}_j\frac{\partial F_j}{\partial y}\right) \tag{42}$$

ENERGY:

$$\rho c_{p_f}\left(u\frac{\partial T}{\partial x} + v\frac{\partial T}{\partial y}\right) = u\frac{dp}{dx} + \mu\left(\frac{\partial u}{\partial y}\right)^2 - \sum_i \dot{w}_i h_i + \sum_i \rho\mathcal{D}_i\frac{\partial F_i}{\partial y}\frac{\partial h_i}{\partial y} + \frac{\partial}{\partial y}\left(k\frac{\partial T}{\partial y}\right) \tag{43}$$

where x is the axial position, y the transverse position (see Figure 16), ρ the density, u the x-component of velocity, v the y-component of velocity, P the pressure, μ the viscosity of the mixture, $\dot{W}_j$ the rate of production of species j, γ_j the diffusivity of specie j into the mixture, F_j the mole-mass ratio of specie j, c_p the specific heat at constant pressure of the mixture, h_i the enthalpy of specie i, and k the thermal conductivity of the mixture. Von Mises transformation for compressible flow was used to simplify the equations for insertion into the code. Introducing the stream function

$$\frac{\partial \psi}{\partial y} = \rho u; \quad \frac{\partial \psi}{\partial x} = -\rho v \tag{44}$$

Equations (41), (42), and (43) become

$$\frac{\partial u}{\partial x} = -\frac{1}{\rho u}\frac{dP}{dx} + \frac{\partial}{\partial \psi}\left(\mu \rho u \frac{\partial u}{\partial \psi}\right) \tag{45}$$

$$\frac{\partial F_j}{\partial x} = \frac{\dot{W}_j}{\rho u} + \frac{\partial}{\partial \psi}\left(\gamma \rho u \frac{\partial F_j}{\partial \psi}\right) \tag{46}$$

$$\frac{\partial T}{\partial x} = \frac{1}{\rho c_p}\frac{dP}{dx} + \mu \rho u\left(\frac{\partial u}{\partial \psi}\right)^2 - \frac{1}{\rho u c_p}\sum \dot{W}_i h_i \tag{47}$$

$$+ \frac{1}{c_p}\left(\sum \gamma \rho u \frac{\partial F_i}{\partial \psi}\frac{\partial h_i}{\partial T}\right) + \frac{1}{c_p}\frac{\partial}{\partial \psi}\left(k \rho u \frac{\partial T}{\partial \psi}\right)$$

The difference equations for Equations (45), (46), and (47) are included in Appendix B.

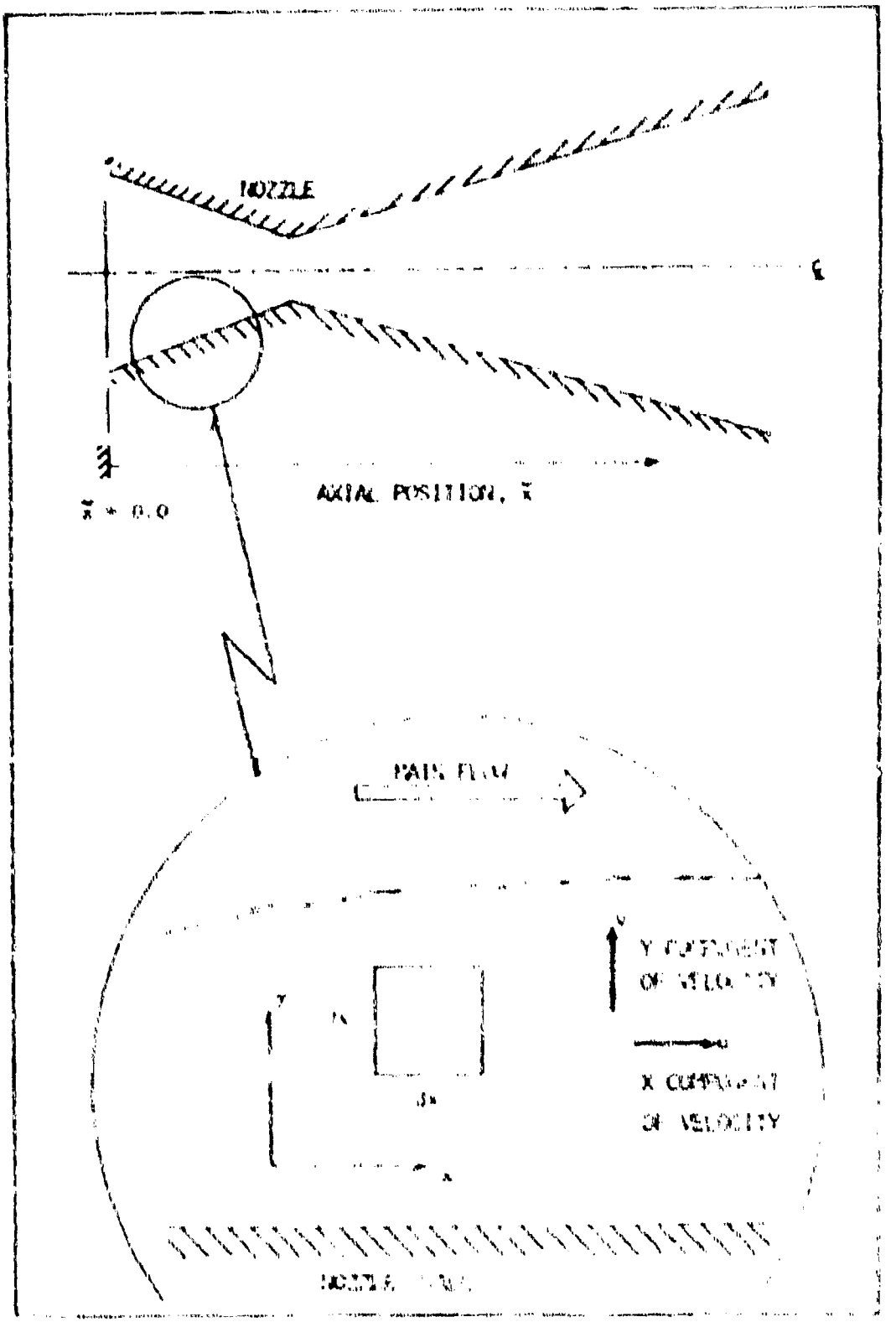

Figure 16. Flow Geometry

Thermodynamic Properties

The enthalpy and specific heat at constant pressure for the individual species were calculated in the form of a quintic polynomial with temperature as the independent variable as follows:

$$\frac{h_i}{R} = aT + \frac{bT^2}{2} + \frac{cT^3}{3} + \frac{dT^4}{4} + e\,\frac{T^5}{5} + f \tag{48}$$

$$\frac{c_{p_i}}{R} = a + bT + cT^2 + dT^3 + eT^4 \tag{49}$$

where the coefficients a, b, c, d, e, and f were taken from Reference 2, and R is the universal gas constant. The density was calculated by

$$\rho = \frac{\bar{P}}{RT\sum_i F_i} \tag{50}$$

Homogeneous Reactions

Two free stream reactions were considered, that of the dissociation of fluorine and that of the recombination of fluorine.

DISSOCIATION

$$F_2 + M \xrightarrow{K_f} 2F + M \tag{51}$$

RECOMBINATION

$$2F + M \xrightarrow{K_b} F_2 + M \tag{52}$$

where M represents any second or third body, respectively. Here the dissociation was defined as the forward reaction. The forward reaction rate used was

$$K_f = 4.2 \times 10^{-11} e^{-(33000/RT)} \tag{53}$$

taken from Reference 5. The backward reaction rate used was

$$K_b = \frac{4.716 \times 10^{15}}{T} e^{(1250/RT)} \tag{54}$$

taken from Reference 28.

Transport Properties

The transport properties for the flow constituents were taken from Reference 29.

VISCOSITY

$$\mu_i = \frac{2.6693 \times 10^{-5} \sqrt{M_i T}}{\sigma_i^2 \Omega_\mu} \tag{55}$$

where Ω_μ is the reduced collision integral curve fit as a function of kT/ϵ_i and M_i is the molecular weight of species i. The values for σ_i, the cross section, and ϵ_i, the

maximum energy of attraction between colliding molecules, were taken from Reference 30. The viscosity for the mixture was calculated using

$$\mu_{MIX} = \sum_{i=1}^{N} \frac{\chi_i \mu_i}{\sum_{i=1}^{N} \chi_j \phi_{ij}} \tag{56}$$

where χ_i is the mole fraction of species i and

$$\phi_{ij} = \frac{1}{\sqrt{8}}\left(1 + \frac{M_i}{M_j}\right)^{-1/2}\left\{1 + \left(\frac{\mu_i}{\mu_j}\right)^{1/2}\left(\frac{M_j}{M_i}\right)^{1/4}\right\}^2 \tag{57}$$

THERMAL CONDUCTIVITY

The thermal conductivity of the flow constituents was calculated using the Eucken approximation

$$k_i = \left(C_{p_i} + \frac{5}{4}\frac{R}{M_i}\right)\mu_i \tag{58}$$

The thermal conductivity of the mixture was calculated by

$$k_{MIX} = \sum_{i=1}^{N} \frac{\chi_i k_i}{\sum_{j=1}^{N} \chi_j \phi_{ij}} \tag{59}$$

where ϕ_{ij} is again given by Equation (57).

DIFFUSIVITY

The diffusivity was calculated by first calculating the binary diffusion coefficient by

$$D_{ij} = \frac{.0018583\sqrt{T^3\left(\frac{1}{M_i}+\frac{1}{M_j}\right)}}{P\,\sigma_{ij}^{2}\,\Omega_D} \tag{60}$$

Ω_D was curve fit as a function of kT/ϵ_{ij} where

$$\epsilon_{ij} = (\epsilon_i\epsilon_j)^{1/2} \tag{61}$$

and σ_{ij} was given by

$$\sigma_{ij} = (\sigma_i + \sigma_j)/2 \tag{62}$$

For calculating the diffusivity of the constituent into the mixture the following scheme was used:

Two Species

$$D_{im} = D_{ij} \tag{63}$$

Three Species

$$D_{1m} = \frac{D_{13}D_{12}(1-x_1) - x_1D_{12}D_{23}\frac{dx_2}{dx_1} - x_1D_{13}D_{23}\frac{dx_3}{dx_1}}{x_1D_{23} + x_2D_{13} + x_3D_{12}} \tag{64}$$

with similar equations for D_{2m} and D_{3m} (Ref 31)

More Than Three Species

For more than 3 species only trace species were handled. When more than 3 species were present, the first 3 were given by Equation (64) and the remaining trace species by

$$D_{im} = \left[\sum_{j=1}^{N} \frac{x_j}{D_{ij}}\right]^{-1} (1 - x_i) \qquad (65)$$

Boundary Conditions

The no slip wall condition for velocity was used. The temperature at the wall was specified either as some constant value or as a function of position along the wall. The wall conditions for concentration of atomic and molecular fluorine were given as follows as a function of the recombination coefficient (derivation included in Appendix C).

$$\frac{(n_i)_{WALL}}{(n_F)_{CELL\ 2}} = \frac{1}{1 + \frac{\sum v_i}{D_F} \left(\frac{kT}{2\pi m}\right)^{1/2}} \qquad (66)$$

where the cell 2 fluorine concentration $(n_F)_{CELL\ 2}$ was calculated prior to CELL 1 (see Figure 17 for nomenclature). Since the code was explicit, calculation of $(n_F)_{CELL\ 2}$ depended only on values at the upstream positions. The

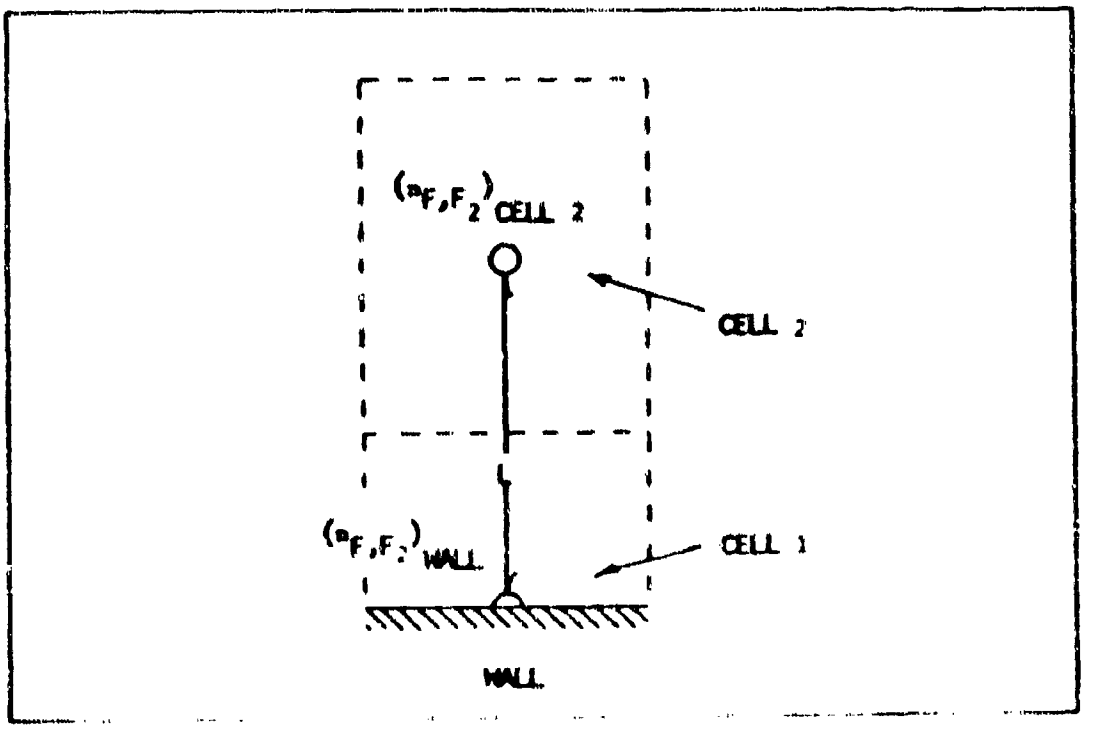

Figure 17. Boundary Condition Nomenclature

quantity L was the vertical distance from the wall to the center of CELL 2. Similarly, F_2 concentrations were calculated by

$$(n_{F_2})_{WALL} = \frac{(n_F)_{WALL}}{D_{F_2}} L\left(\frac{kT}{2\pi m}\right)^{1/2} + (n_{F_2})_{CELL\ 2} \qquad (67)$$

The nozzle centerline conditions were handled by symmetrical reflection.

The domain of the calculation was from an axial position, $\tilde{x} = 0.0$ at the nozzle entrance to $\tilde{x} = 0.4$ at the nozzle exit (see Figure 16).

Results of Nozzle Flow Computations

The boundary layer code was run for predictions of the effects of recombination on laser nozzle flow. The pressure profile and nozzle contour for a representative slit nozzle are given in Figure 18 (taken from Ref 4). While not the most commonly used slit nozzles, it was similar in size and basic contour. The input conditions for these computations are given in Table III.

Computations were run for three wall catalytic conditions: (1) noncatalytic wall, $\gamma = 0.0$, (2) fully catalytic, $\gamma = 1.0$ (Ferrell et.al. conditions) and (3) step by step computation of γ based upon the recombination model. The results are presented in Figures 19 through 28. These results, as mentioned previously, were based on the assumption of laminar flow. The highest Reynolds number based on the momentum thickness was approximately 65. This was well within the laminar regime as transition to turbulence occurs at around 360 (Ref 32).

Velocity. Figures 19 and 20 show the effect the recombination had on the velocity profile at the throat and exit plane respectively. As can be seen there was no

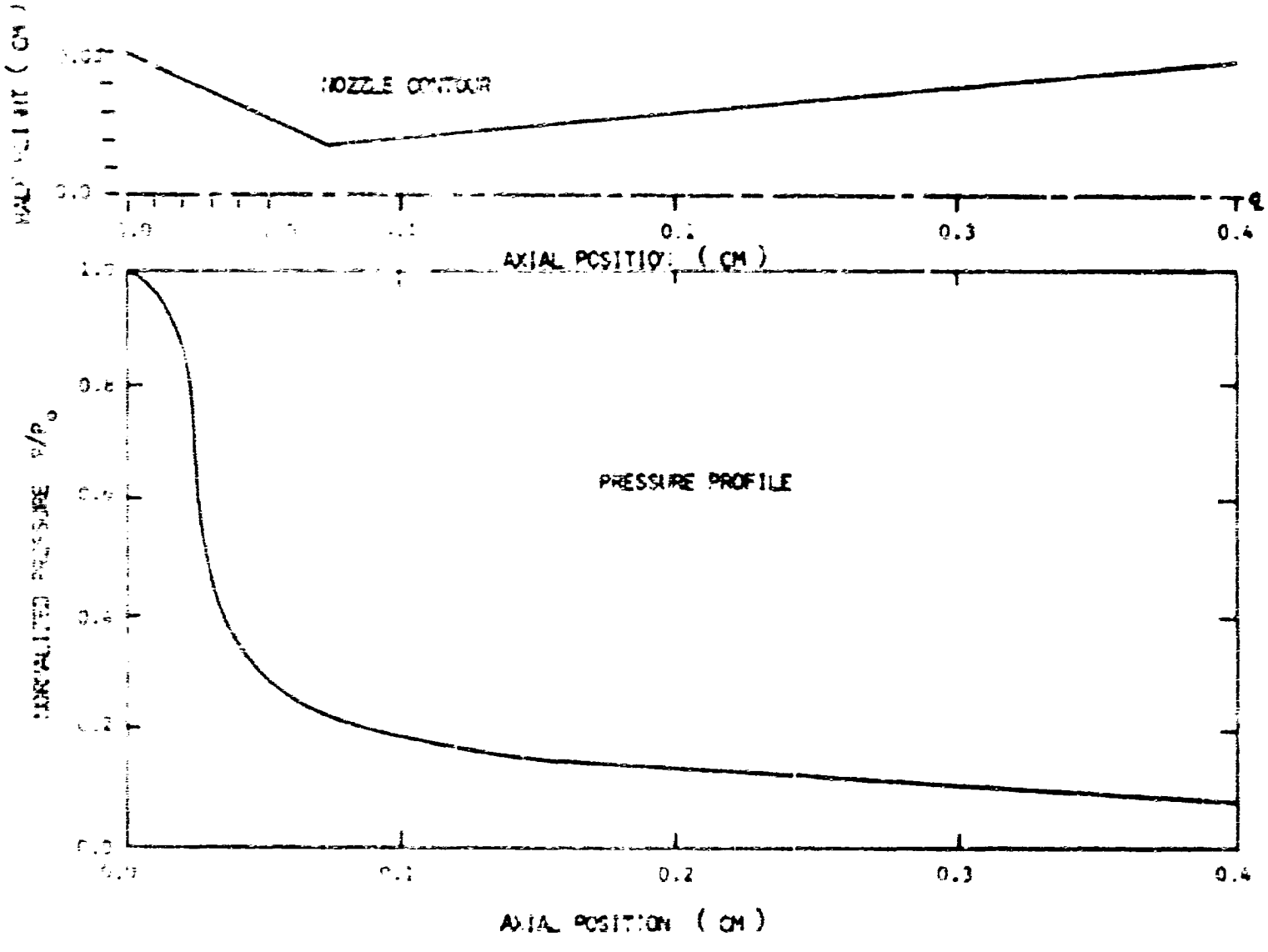

Figure 18. Nozzle Contour and Pressure Profile

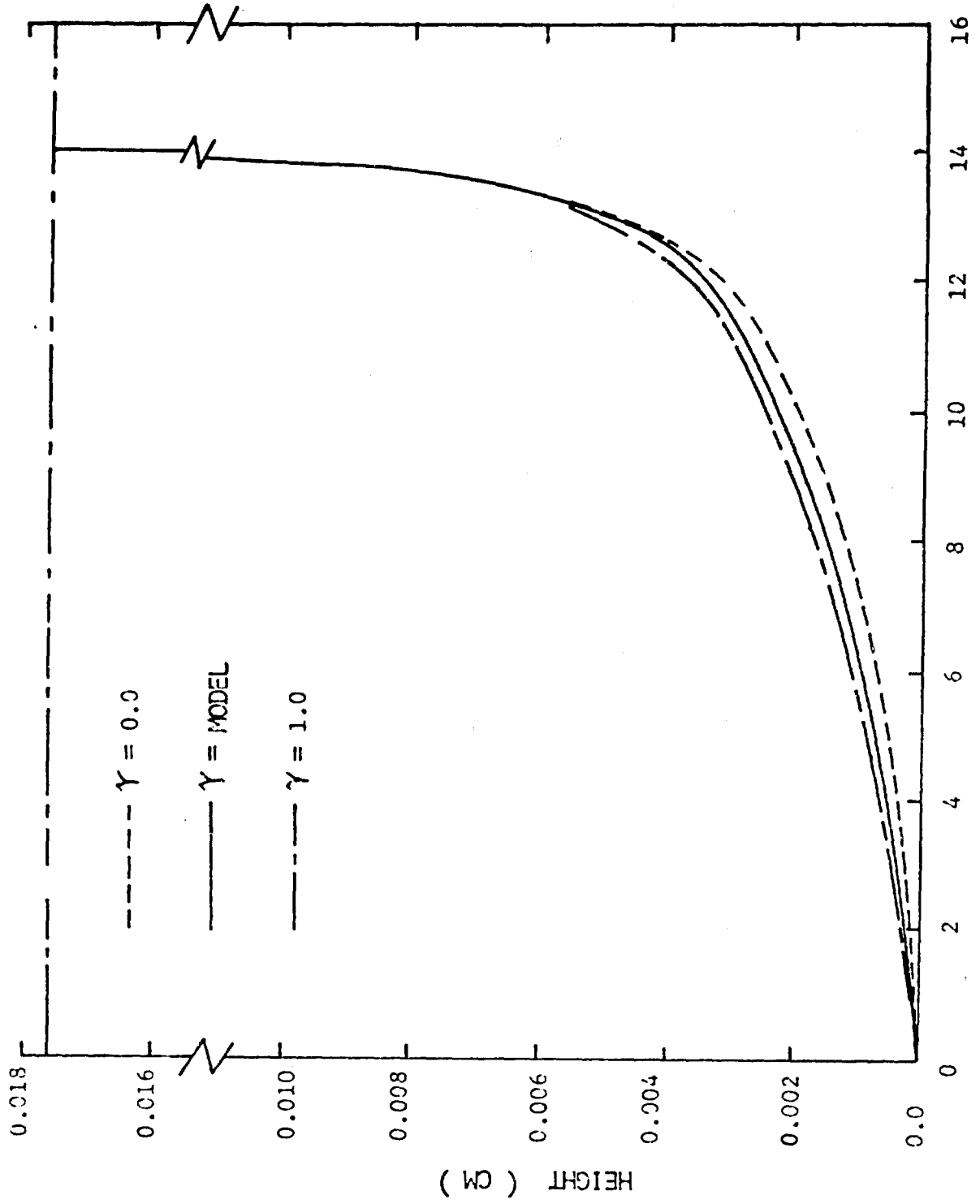

Figure 19. Velocity Profile at Throat

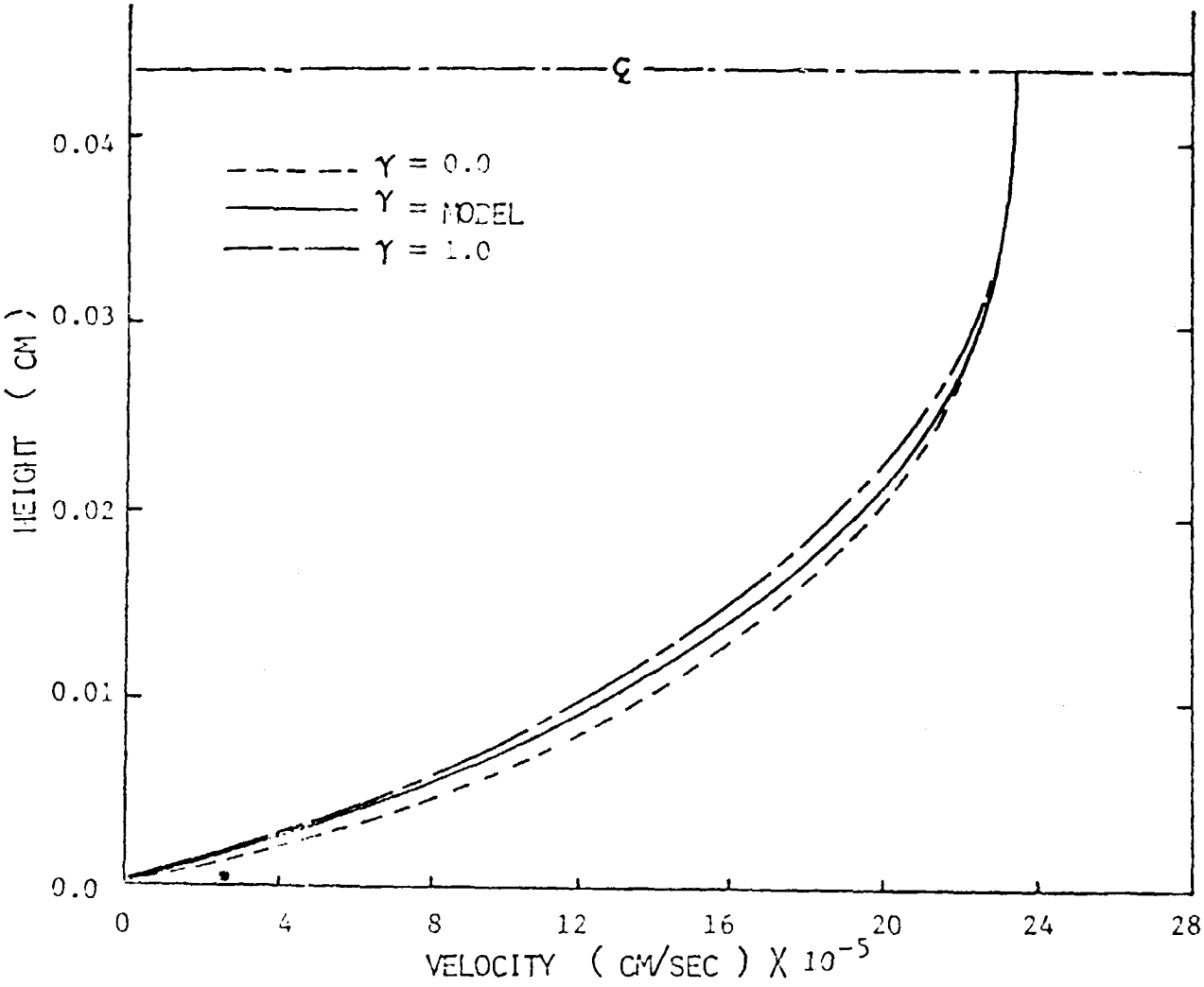

Figure 20. Velocity Profile at Exit Plane

major difference in the velocity profiles, only a slight lessening of the velocity gradient at the wall with recombination, decreasing the most for the case where $\gamma = 1.0$.

Temperature. Figures 21 and 22 show the effect the recombiantion had on the temperature profiles at the throat and exit plane, respectively. The throat profile showed very little change with only a slight steepening in the temperature gradient at the wall with increasing recombination. The exit plane profile, however, showed a more dramatic effect both in an increasing slope at the wall and a shifting of the profile near the boundary layer mid-portion.

The overall wall effect appeared to be a slightly increased heat transfer to the wall due to normal conductive heat transfer (see Figure 22). To this should be added the heat released in the recombination reaction. For this case the temperature was assumed constant along the wall as indicated in Table III, but an actual determination of the nozzle wall temperature profile should not neglect the role of the energy of the reaction. This energy is dumped directly into the wall as indicated by Meyerson (Ref 33) prior to being either conductively carried away by the wall or recoupled into the flow through normal heat transfer processes. This additional heat transfer turns

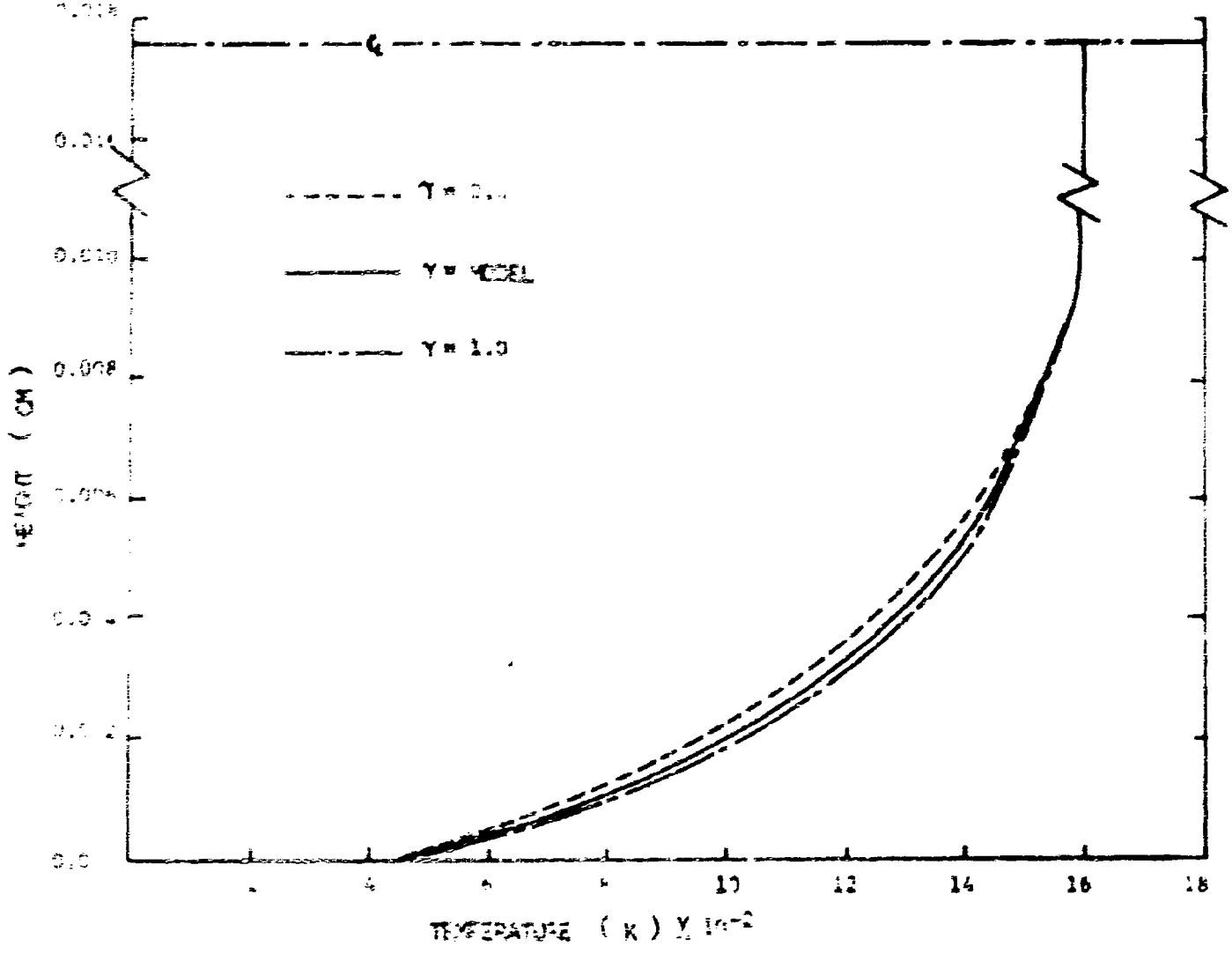

Figure 21. Temperature Profile at the Throat

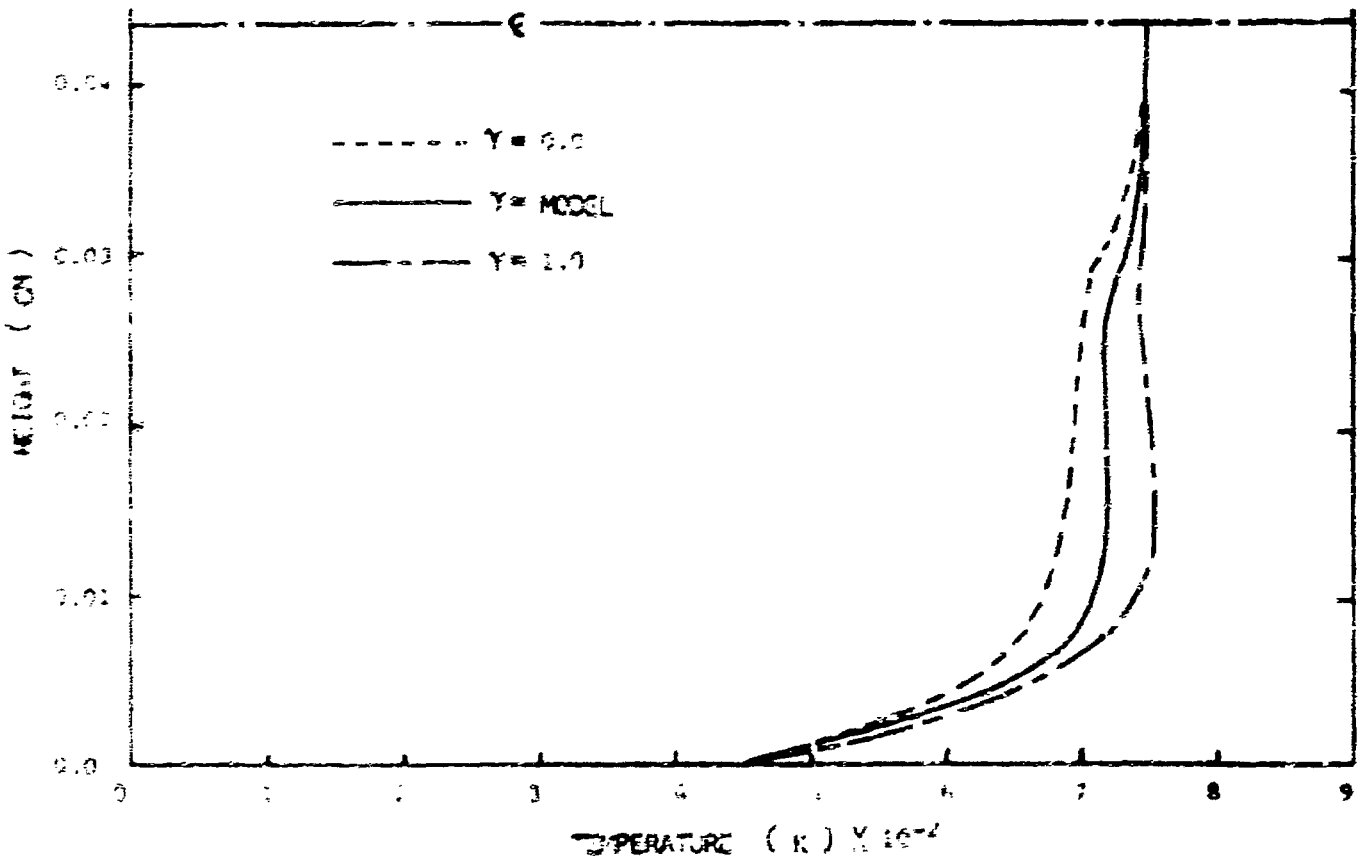

Figure 22. Temperature Profile at the Exit Plane

out to be significant, up to three times the normal conduction as can be seen in Figure 23.

Table III. Input Conditions

PARAMETER	VALUE
VELOCITY	$3.1 \times 10^4 \frac{cm}{sec}$
PRESSURE	760 TORR
MOLE FRACTIONS	
[F]	0.272
$[F_2]$	0.00035
[He·HF]	0.728
TEMPERATURE	
GAS	2000 K
WALL	450 K (CONSTANT)

The effect on the mid-boundary layer portion of the profile is interesting and could be important in laser cavity computations. The typical viscous heating distortion of the profile as indicated by the noncatalytic curve in Figure 22, is affected by the diffusion of F and F_2. While the mass diffusive flux was balanced, the higher enthalpy of two F atoms as compared to one F_2 molecule tended to draw energy out of the midstream thereby smoothing out the profile.

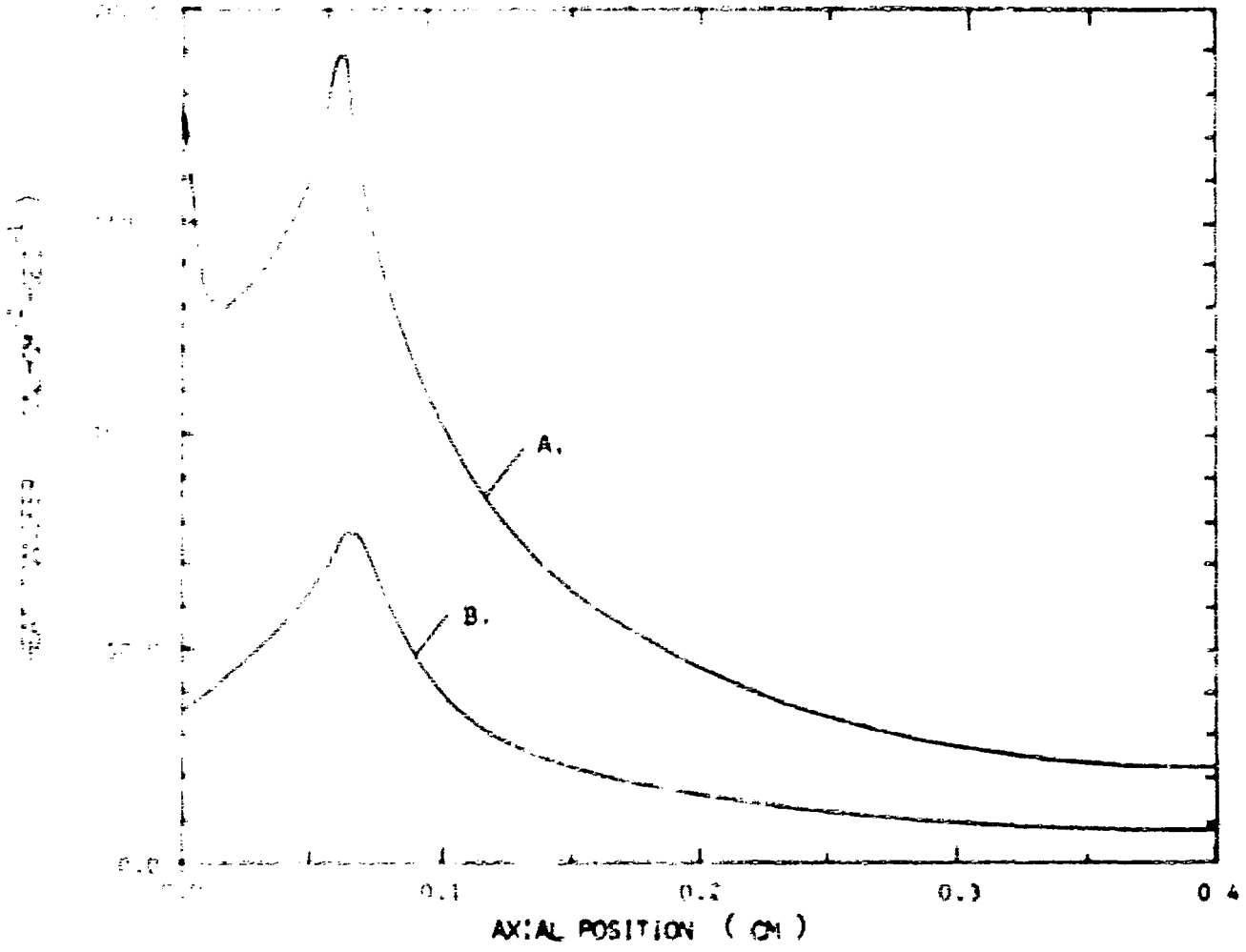

Figure 23. Heat Transfer to Nozzle Wall
A. Total Heat Transfer to Wall Including Heat of Reaction
B. Heat Transfer Due to Normal Heat Transfer

Chemical Constituents The effect of recombination on the concentration profiles was of most interest and is examined in Figures 24 through 28. Figures 24 and 25 give the profiles at the throat and exit plane, respectively; Figure 26 shows the depletion of F and growth of F_2 with axial position along two stream functions in the nozzle; Figure 27 shows the loss of F, and Figure 28 contains the recombination coefficient as a function of axial position. Although Figures 24 and 25 show a difference between the fully catalytic versus the model, it is noticeably less of a difference than the one and a half order of magnitude difference in the recombination coefficients (see Figure 28). The reason for this can be found by analysis of the boundary conditions given earlier in this section.

The flux of F atoms recombining at the wall is given by

$$\dot{c} = 2\gamma(\rho_F)_w k_w (\rho_F)_w^{1/2} \qquad (68)$$

Using the boundary conditions, Equation (66), Equation (68) becomes:

$$\dot{c} = \frac{2\gamma_{\cdots}(\rho_{\cdots})_{\cdots}\,k_{\cdots}\,(\rho_{\cdots})_{\cdots}^{1/2}}{1 + \frac{2\gamma_{\cdots}k_{\cdots}}{\beta_{\cdots}}\left(\frac{\rho_{\cdots}}{\rho_{\cdots}}\right)^{1/2}} \qquad (69)$$

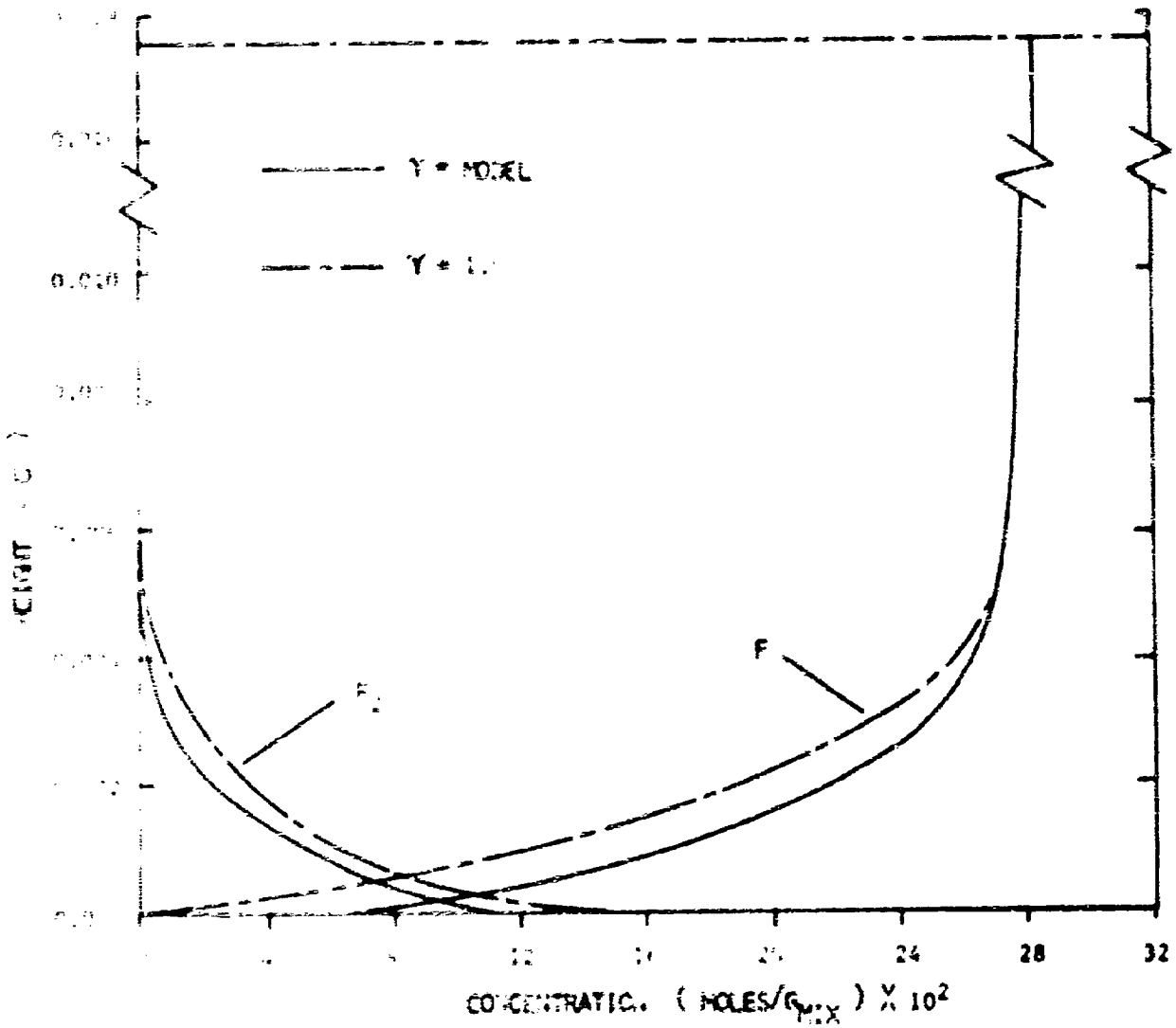

Figure 24. Concentration Profiles at Throat

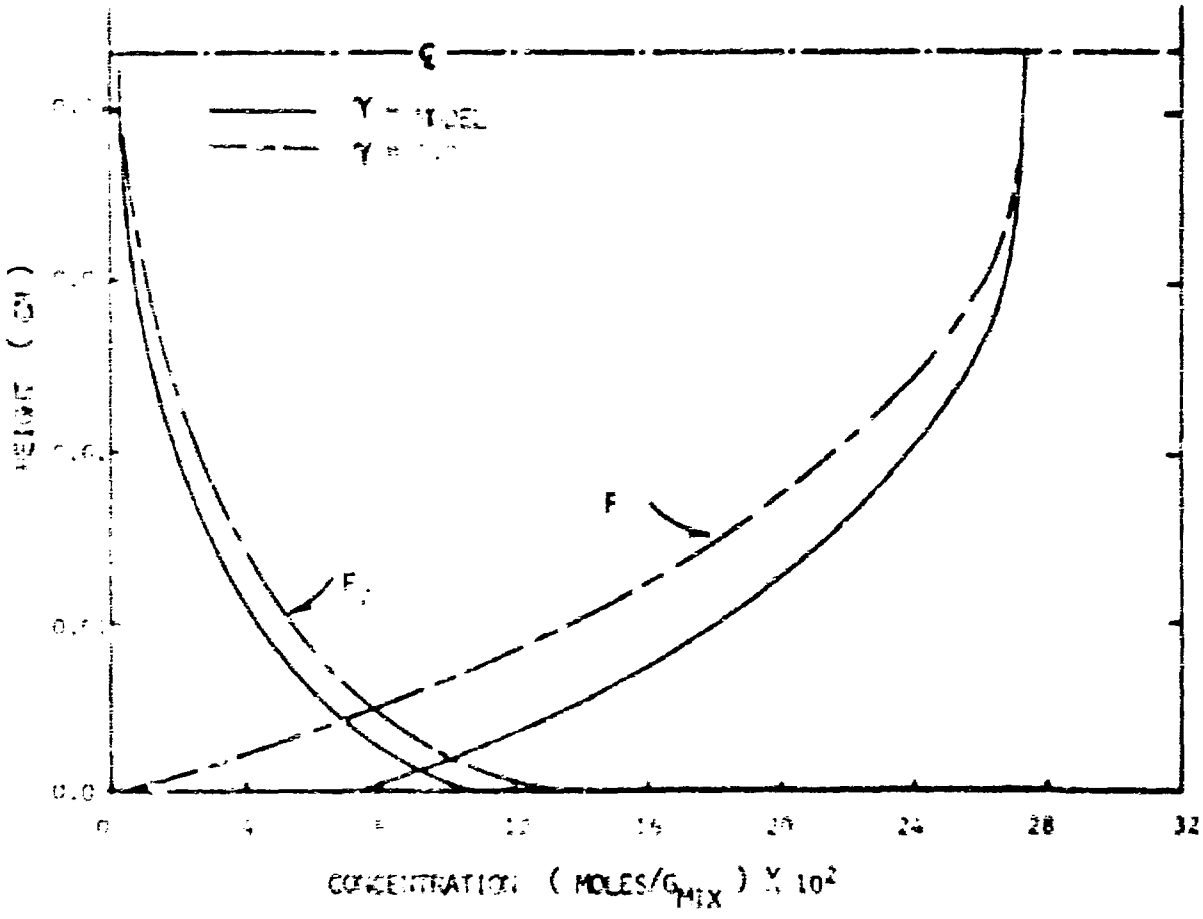

Figure 25. Concentration Profiles at Exit Plane

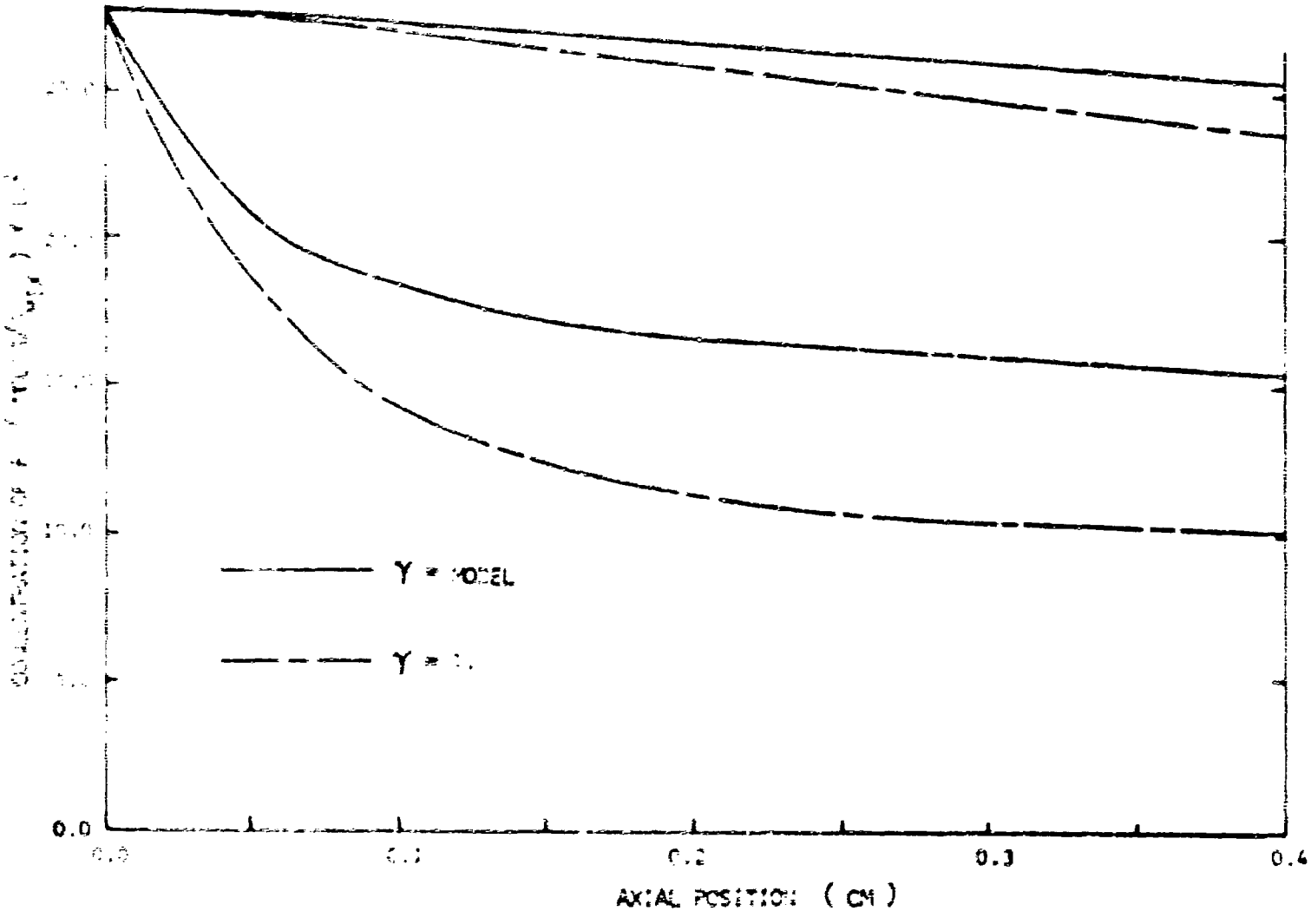

Figure 26. Depletion of F Concentration for Two Stream Tubes
LOWER: Stream Tube Near Wall
UPPER: Stream Tube Midway Between Wall and Centerline

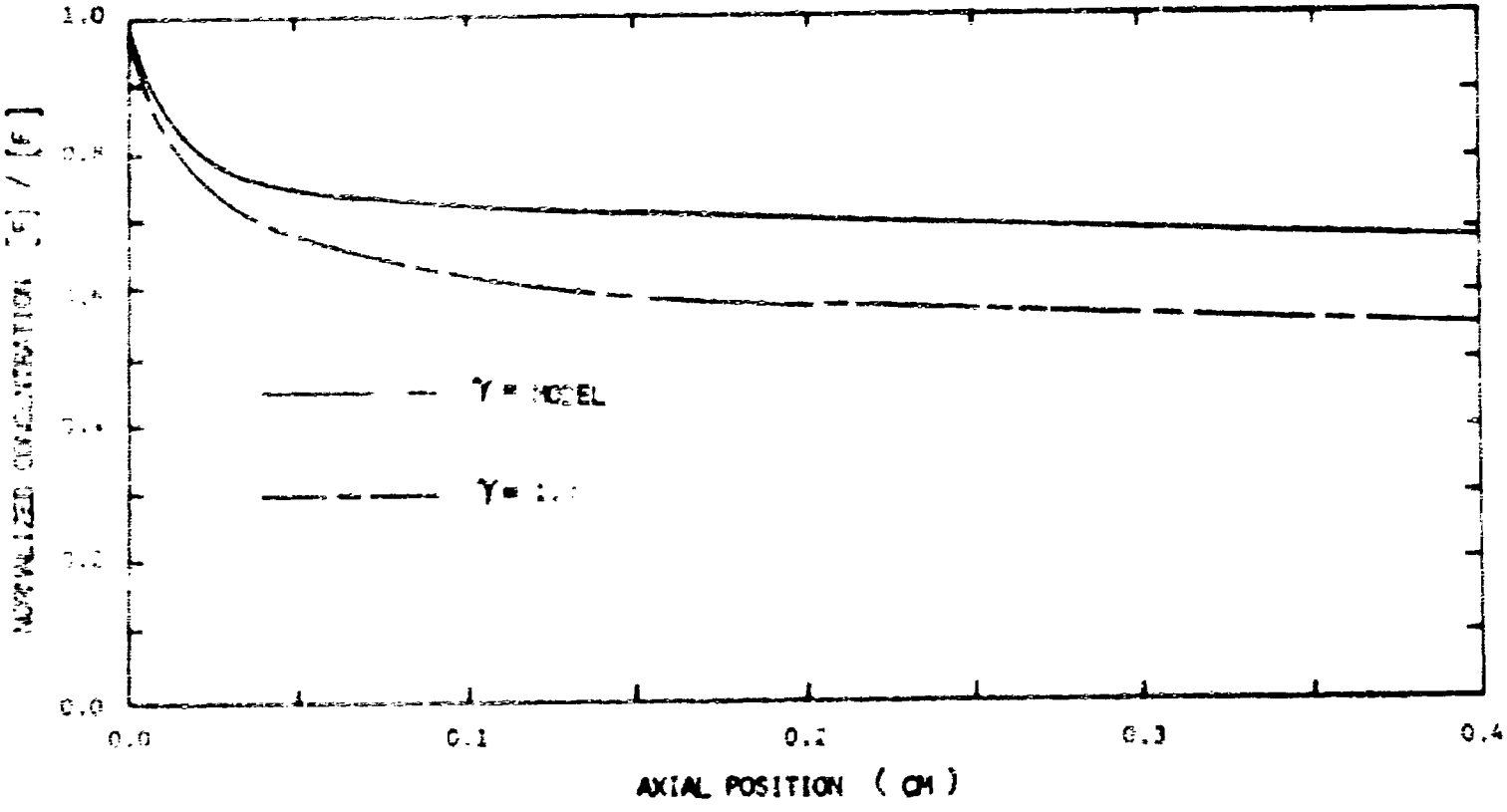

Figure 27. Depletion of F Integrated Over Entire Flow

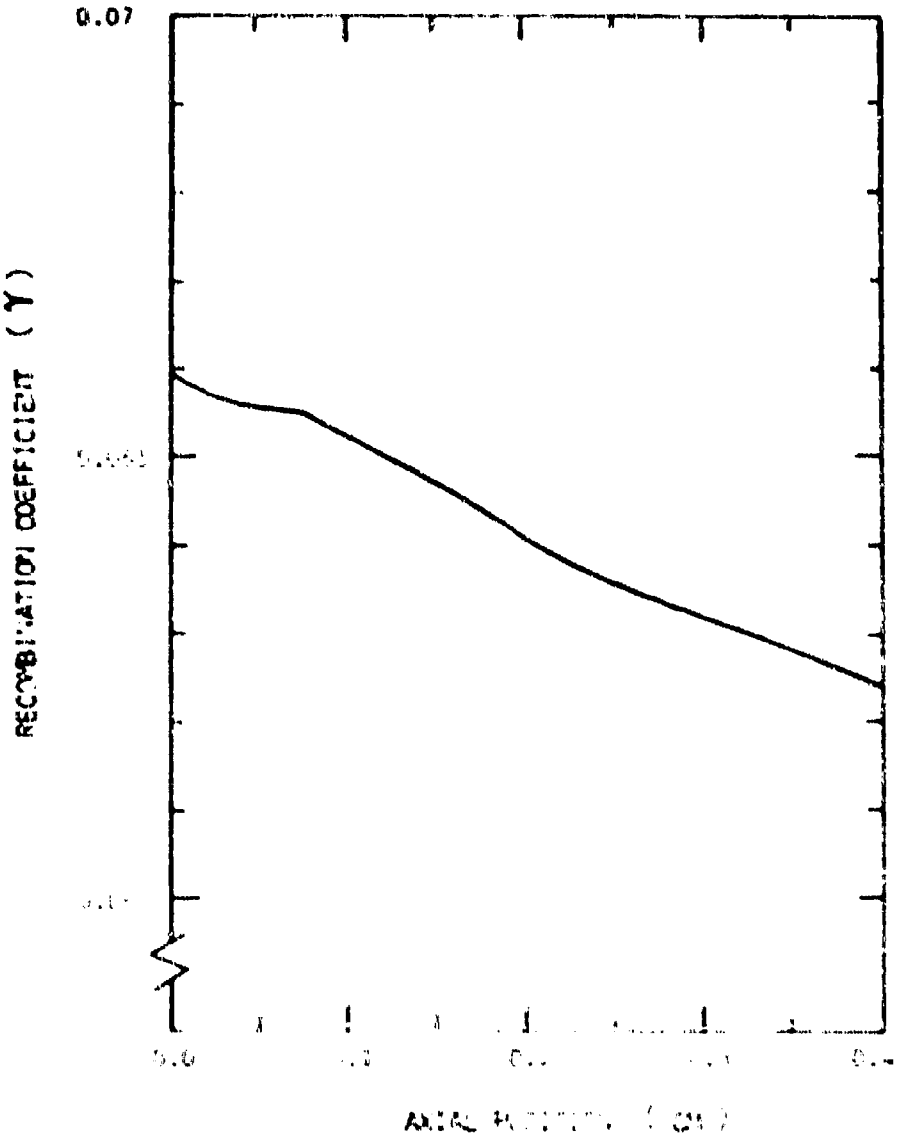

Figure 25. Wall Recombination Coefficient

Finally, rearranging the terms slightly

$$\phi = \frac{2(n_F)_{CELL\ 2}}{\frac{1}{\gamma\left(\frac{RT}{2\pi m}\right)^{1/2}} + \frac{2L}{\mathcal{D}_F}} \qquad (70)$$

Thus, the actual rate at which F is depleted from the system is dependent on both the diffusivity and the recombination coefficient. Examination of the two terms in the denominator of Equation (70) yields the figures in Table IV. The table shows that while the γ's differed by 17, the actual depletion was limited to a difference of only 5 at the exit and 4 at the throat due to only the terms in the denominator of Equation (70). Coupled to this limiting influence, the actual F atom concentration in CELL 2 limited still further the difference in the two solutions so that the final differences were reduced from 17 to approximately 1.4. This ratio is verified by Figure 27, where the total amount of atomic fluorine removed by recombination was 32 percent compared with 45 percent removed when $\gamma = 1.0$.

Table IV. Flux Denominator

		$\gamma = 1.0$	$\gamma = MODEL$
$\frac{1}{\gamma\left(\frac{2}{\gamma+1}\right)^{1/2}}$	THROAT	5.65×10^{-5} (sec/cm)	8.60×10^{-4} (sec/cm)
	EXIT PLANE	5.65×10^{-5} (sec/cm)	9.11×10^{-4} (sec/cm)
$\frac{1}{a_T}$	THROAT	1.90×10^{-4} (sec/cm)	1.90×10^{-4} (sec/cm)
	EXIT PLANE	1.41×10^{-4} (sec/cm)	1.50×10^{-4} (sec/cm)
ρ_T	THROAT	1.032×10^{-2} (MOLES/cm^3)	5.580×10^{-3} (MOLES/cm^3)
	EXIT PLANE	1.210×10^{-2} (MOLES/cm^3)	3.601×10^{-3} (MOLES/cm^3)

VI. Conclusions and Recommendations

The present work dealt with the construction of a theoretical model for the heterogeneous recombination reaction of fluorine at a metal surface. Using the Rideal mechanism the reaction was divided into three distinct processes (1) the bonding process of atomic fluorine to the wall, (2) the collision and recombination process of a gas-phase fluorine atom and a bonded fluorine atom and (3) the rate process at which the bonding and recombination takes place considering the surface coverage. Having treated each of the processes in some detail, these processes were combined to form the final wall recombination model. The model was adapted to one-dimensional pipe flow and computations made for comparison with data taken by Dr. Casper J. Hitee / United Aircraft Research Laboratories. Finally the model was placed into a two-dimensional, steady state, laminar boundary layer code to demonstrate the effect one might expect from "real" fluorine wall recombination in regards of the kind found in fluorine chemical lasers.

The model was found to describe the available experimental data, shedding insight into how the controlling process vary as a function of temperature. Analysis of the argon-fluorine experiment indicated three distinct regimes

(1) a low temperature regime (less 350 K) in which the recombination reaction was poisoned by argon dominating the surface, (2) a mid-temperature regime (350 K to 475 K) in which the argon was thermally desorbed and the fluorine thermal desorption was not significant enough to substantially decrease the surface coverage of fluorine and (3) a high temperature regime (475 K to [illegible] K) in which thermal desorption played a significant role in decreasing the fluorine surface coverage. While the effect of other diluents on the first regime is speculative, it is predicted, based on computations contained herein, that the recombination coefficient would be significantly higher in the low temperature regime with a helium diluent. The third regime, however, was found to be purely a property of the fluorine-surface system and it is clear that the recombination process is greatly decreased by maintaining the surface temperature above 500 K for total pressure of 2.7 torr. Temperatures above 500 K were not treated; near 600 K one can expect to see the maximum recombination rate.

The effect of realistic recombination rates predicted by the model on laser gain was found to be quite significant. While the velocity profiles were nearly unchanged, the temperature and concentration profiles were changed significantly. Temperature profiles can be expected to be shifted from those of noncatalytic profiles due to the influence of the diffusion of F and F_2 through the flow.

The concentration profiles of I and I_2, while expected to be [illegible] of the [illegible] profile [illegible] change [illegible] effect. [illegible] predicted that at 450 A [illegible] will be [illegible] approximately [illegible] 27 [illegible] [illegible] every [illegible] [illegible] 22 percent of the total [illegible] would be [illegible]

[illegible]

run by Ultee should be run with a helium diluent to fully verify the insignificance of F_2 attachment. Additionally, future efforts should be addressed to the problem of interfacing this model with production flow codes designed specifically for analysis of chemical laser nozzles such as the one described in Reference 2.

Bibliography

1. [illegible] Research." Proceedings of the IEEE, Vol 61, p. 414 (April 1973).

2. Brooks, F. P. "Development of Chemical Based Computer Models." AIAA 58-1048 (July 1958).

3. "Laser Analysis and Review." Presentation to the Air Force [illegible] Laboratory Director's for Advanced Technology Systems [illegible], Conducted by Aerospace Company, Huntsville, Alabama, [illegible].

4. [illegible]

5. [illegible]

Bibliography

12. Valance, W., Birang, B., and Maclean, D. I. "Measurement of Fluorine Atom Concentrations and Recombination Rates by ESR Spectroscopy." FRK-116, Department of Chemistry, Boston College, Chestnut Hill, Massachusetts (October 1971).

13. Ultee, Casper, J., Private Communications.

14. Vincenti, W. G., and Kruger, C. H. Introduction to Physical Gas Dynamics, New York, Wiley (1967).

15. Lennard-Jones, J. E. "Processes of Adsorption and Diffusion on Solid Surfaces." Trans. Faraday Society, No. 28, p. 334 (1932).

16. Weast, R. C. Handbook of Chemistry and Physics (53rd Edition), Cleveland, Chemical Rubber Publishing Company (1972).

17. Bardeen, J. "The Image and Van der Waal Forces at a Metallic Surface." Physical Review, Vol 58, p. 727 (October 1940).

18. Margenau, H., and Pollard, W. G. "The Forces Between Neutral Molecules and Metallic Surfaces." Physical Review, Vol 60, p. 128 (July 1941).

19. Prosen, E. J. R., and Sachs, R. G. "The Interaction Between a Molecule and a Metal Surface." Physical Review, Vol 61, p. 65 (January 1942).

20. Mavroyannis, C. "The Interaction of Neutral Molecules with Dielectric Surfaces." Molecular Physics, 6, p. 593 (1963).

21. Logan, R. M., and Keck, J. C. "Classical Theory for the Interaction of Gas Atoms with Solid Surfaces." Journal of Chemical Physics, Vol 49, No. 2 p. 860 (July 1968).

22. Pagni, P. J., and Keck, J. C. "Diffusion Theory for Adsorption and Desorption of Gas Atoms at Surfaces." The Journal of Chemical Physics, Vol 50, No. 3, p. 1162 (February 1973).

23. Modak, A. T., and Pagni, P. J. "Atom Trapping on Surfaces." The Journal of Chemical Physics, Vol 59, No. 4, p. 2019 (August 1973).

Bibliography

24. Christmann, K., Schober, O., Ertl, G., and Neumann, M. "Adsorption of Hydrogen on Nickel Single Crystal Surfaces." The Journal of Chemical Physics, Vol 60, No. 11, p. 4528 (June 1974).

25. Glasstone, S., Laidler, K. J., and Eyring, H. Theory of Rate Processes. New York, McGraw-Hill (1941).

26. Van der Ziel, A. Solid State Physical Electronics. Englewood Cliffs, New Jersey, Prentice-Hall (1957).

27. Smith, W. V. "The Surface Recombination of H Atoms and OH Radicals." Journal of Chemical Physics, Vol 11, p. 110 (March 1943).

28. Kurzius, S. C. "Lamp Reaction Models for Analysis of Chemical Lasers." TR-RK-CR [illegible] Vol III, Propulsion Directorate, U.S. Army Missile Research, Development and Engineering Laboratory, Redstone Arsenal, Alabama (June 1975).

29. Hirschfelder, J. O., Curtiss, C. F., and Bird, R. B. Molecular Theory of Gases and Liquids. New York, Wiley (1954).

30. Svehla, R. A. "Estimated Viscosities and Thermal Conductivities of Gases at High Temperatures." NASA TR-R-132, National Aeronautics and Space Administration (1962).

31. Mickley, H. S., Ross, R. C., Squyers, A. L., and Stewart, W. E. "Heat Mass and Momentum Transfer for Flow over a Flat Plate with Blowing or Suction." NACA-TN-3208, National Advisory Committee for Aeronautics (1954).

32. Kays, W. M. Convective Heat and Mass Transfer. San Francisco, McGraw-Hill (1966).

33. Myerson, A. L. "Mechanisms of Surface Recombination From Step Function Flows of Atomic Oxygen Over Noble Metals." Journal of Chemical Physics, Vol 42, No. 9, p. 3270 (May 1965).

Appendix A

Solution of the Equations of Motion for the Gas-Wall Collision Model

The gas-wall collision system, as shown in Figure A.1, is analyzed as follows.

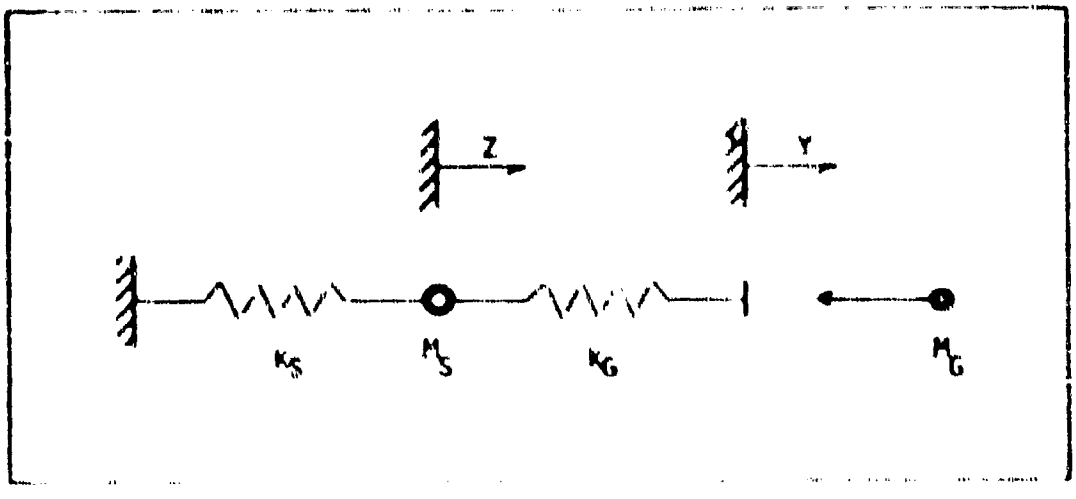

Figure A.1. Gas-Wall Collision System

At the instant the collision begins, the equations of motion become

$$m_S\ddot{Z} + (k_g + k_s)\,Z - k_g Y = 0 \qquad (A.1)$$

$$m_g\ddot{Y} - k_g Z + k_g Y = 0 \qquad (A.2)$$

The solution of Equations (A.1) and (A.2) proceeds as follows: The solution for Y and Z is assumed to have the form

$$Y(t) = A \sin(\omega t) \tag{A.3}$$

$$Z(t) = B \sin(\omega t) \tag{A.4}$$

In the usual manner, the assumed solutions are differentiated for the first and second derivatives and the results substituted into Equations (A.1) and (A.2). The result can be expressed in matrix form by

$$\begin{bmatrix} (-m_g\omega^2 + k_g) & -k_g \\ -k_g & (-m_s\omega^2 + (k_g + k_s)) \end{bmatrix} \begin{bmatrix} A \\ B \end{bmatrix} = 0 \tag{A.5}$$

Thus for a non-trivial solution of A and B the matrix on the left must be singular. Setting the determinant to zero

$$m_g m_s(\omega^2)^2 - (m_s k_g + m_g k_s + m_s k_g)\omega^2 + k_g k_s = 0 \tag{A.6}$$

Solving for the roots of Equation (A.6)

$$\omega_{1,2} = \left\{ \frac{(m_g k_g + m_g k_s + m_s k_g) \pm \sqrt{(m_g k_g + m_g k_s + m_s k_g)^2 - 4 m_g m_s k_g k_s}}{2 m_s m_g} \right\}^{1/2} \tag{A.7}$$

where ω_1 refers to the solution of ω with the + and ω_2 refers to the solution of ω with the -. The amplitude ratio equation is given by

$$(m_B\omega^2 + k_B)A - k_B B = 0 \qquad (A.8)$$

which gives the following amplitude ratios

$$\left(\frac{A}{B}\right)_{1,2} = \frac{k_B}{k_B - m_B(\omega_{1,2})^2} \qquad (A.9)$$

Thus the general solution of Equations (A.1) and (A.2) is given by

$$X(t) = A_1\sin(\omega_1 t + \phi_1) + A_2\sin(\omega_2 t + \phi_2) \qquad (A.10)$$

$$Z(t) = B_1\sin(\omega_1 t + \phi_1) + B_2\sin(\omega_2 t + \phi_2) \qquad (A.11)$$

Equations (A.10) and (A.11) leave 4 independent unknowns which are solved for using the initial conditions

$$Y(0) = \dot{Y}(0) = \varepsilon\sin\phi \qquad (A.12)$$

where ϕ is the initial phase angle and ε is the amplitude of surface atom oscillation.

Also,

$$\dot{Z}(0) = \omega_s \cos\phi \tag{A.13}$$

$$\dot{Y}(0) = \left(\frac{2\epsilon}{m}\right)^{1/2} \tag{A.14}$$

where ϵ is the energy

$$\epsilon = \frac{1}{2}m\left(V_s + \sqrt{\frac{2AF_w(R_E)}{m_R}}\right)^2 \tag{A.15}$$

as indicated in Equation (17) of the main text.

Let the amplitude ratios from Equation (A.9) be defined as follows

$$C_1 = \frac{A_1}{R_1} \tag{A.16}$$

$$C_2 = \frac{A_2}{R_2} \tag{A.17}$$

Then the result of using the initial conditions yields the solutions

$$Y(t) = (A_1\cos\phi_1)\sin\omega_1 t + (A_1\sin\phi_1)\cos\omega_1 t$$

$$+ (A_2\cos\phi_2)\sin\omega_2 t + (A_2\sin\phi_2)\cos\omega_2 t \tag{A.18}$$

$$z(t) = \frac{1}{C_1}\{(A_1\cos\phi_1)\sin\omega_1 t + (A_1\sin\phi_1)\cos\omega_1 t\} + \frac{1}{C_2}\{(A_2\cos\phi_2)\sin\omega_2 t + (A_2\sin\phi_2)\cos\omega_2 t\} \tag{A.19}$$

$$\dot{Y}(t) = \omega_1(A_1\cos\phi_1)\cos\omega_1 t - \omega_1(A_1\sin\phi_1)\sin\omega_1 t + \omega_2(A_2\cos\phi_2)\cos\omega_2 t - \omega_2(A_2\sin\phi_2)\sin\omega_2 t \tag{A.20}$$

where

$$A_1\sin\phi_1 = z(0)\left\{\frac{\frac{1}{C_2} - 1}{\frac{1}{C_2} - \frac{1}{C_1}}\right\} \tag{A.21}$$

$$A_2\sin\phi_2 = z(0)\left\{\frac{1 - \frac{1}{C_1}}{\frac{1}{C_2} - \frac{1}{C_1}}\right\} \tag{A.22}$$

$$A_1\cos\phi_1 = \left(\frac{1}{\omega_1}\right)\left\{\frac{\frac{1}{C_2}\dot{Y}(0) - \dot{z}(0)}{\frac{1}{C_2} - \frac{1}{C_1}}\right\} \tag{A.23}$$

$$A_2\cos\phi_2 = \left(\frac{1}{\omega_2}\right)\left\{\frac{\dot{z}(0) - \frac{1}{C_1}\dot{Y}(0}{\frac{1}{C_2} - \frac{1}{C_1}}\right\} \tag{A.24}$$

The results of computations made from Equations (A.18), (A.19), and (A.20) for a temperature of 300 K and an incoming non-dimensional velocity

$$\frac{V_3}{\sqrt{\frac{2kT}{m_F}}} = 0.3 \qquad (A.25)$$

for fluorine on copper is given in Figure A.2. Examination of Figure A.2 shows that for a non-dimensional initial velocity of 0.3 the probability of being trapped (represented by L_1/L_2 in Figure A.2) is 50 percent.

Computations made for a range of initial velocities yields Figure A.3 (note in Figure A.3 that the probability corresponding to an initial non-dimensional velocity of 0.5 is 0.5).

A family of curves similar to the curve in Figure A.3, for a range of temperatures from 0 K to 800 K and Figure 4 from the main text, combine to yield the curve for the initial sticking coefficient such as the broken line in Figure 9 of the main text for the sticking coefficient of fluorine on copper.

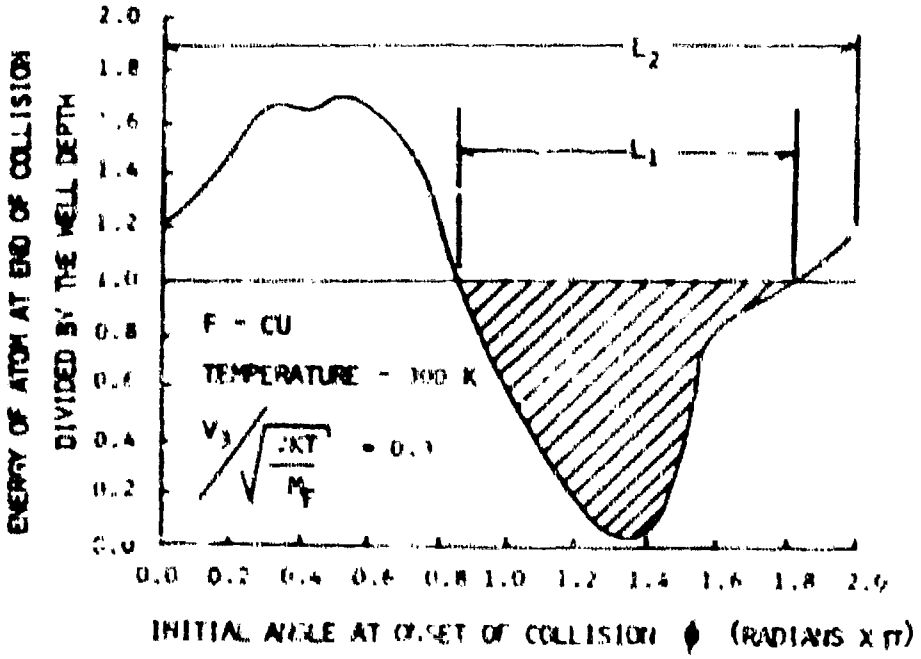

Figure A.2. Initial Angle at Onset of Collision vs. Atom-Out Energy

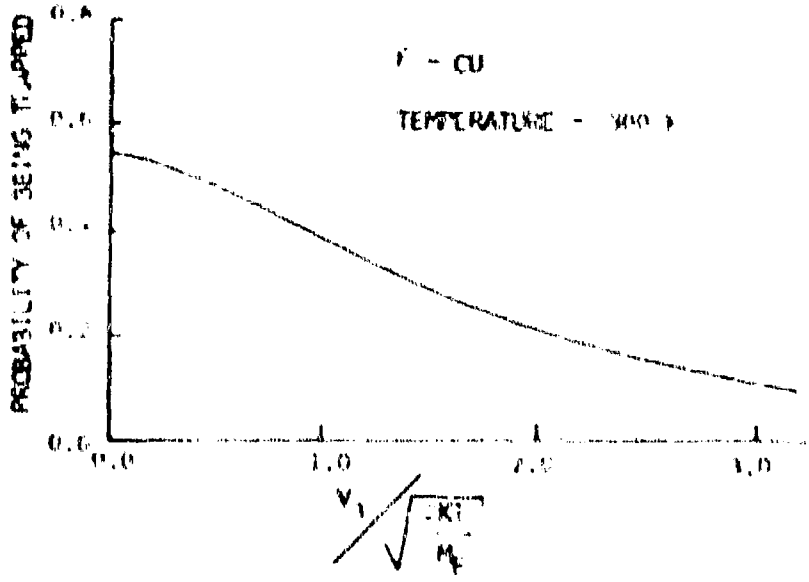

Figure A.3. Probability of Atom Being Trapped

Appendix B

Difference Equations

All functions of x, and ψ were treated as the following fictitious function f(x,ψ) using the cell nomenclature shown in Figure B.1.

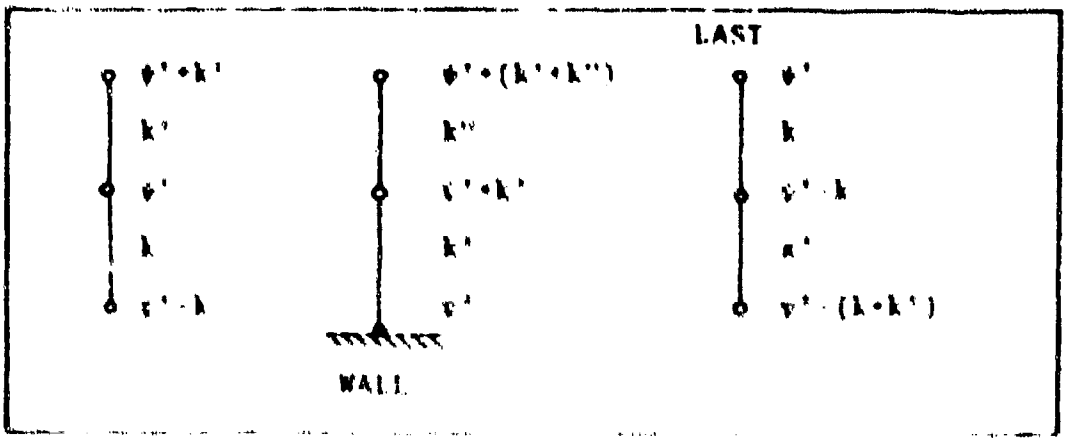

Figure B.1. Cel Nomenclature

First and second derivatives were approximated by

$$\frac{\partial f(x,\psi)}{\partial \psi} \approx \frac{\Delta f(x,\psi)}{\Delta \psi} \qquad (B.1)$$

$$\frac{\partial^2 f(x,\psi)}{\partial \psi^2} \approx \frac{\Delta^2 f(x,\psi)}{\Delta \psi^2} \qquad (B.2)$$

where the Δ operators are defined in the following.

FIRST DERIVATIVE Δ OPERATOR

$$\left.\frac{\Delta f(x,\psi)}{\Delta\psi}\right|_{\psi=\psi'} \equiv \frac{Af(x,\psi_A) - Bf(x,\psi_B) - Cf(x,\psi_C)}{D} \qquad (B.3)$$

where:

for all cells except the wall cell and the last cell

$A = k^2$

$B = k'^2$

$C = k^2 - k'^2$

$D = k^2k' + kk'^2$

$\psi_A = \psi' + k'$

$\psi_B = \psi' - k$

$\psi_C = \psi'$

for the wall cell

$A = (k' + k'')^2$

$B = k'^2$

$C = (k' + k'')^2 - k'^2$

$D = k'^2k'' + k'k''^2$

$\psi_A = \psi' + k'$

$\psi_B = \psi' + (k' + k'')$

$\psi_C = \psi'$

for the last cell

$A = k^2$

$B = (k + k')^2$

$$C = k^2 - (k + k')^2$$

$$D = k^2k' + kk'^2$$

$$\psi_A = \psi' - k$$

$$\psi_B = \psi' - (k + k')$$

$$\psi_C = \psi'$$

SECOND DERIVATIVE Δ OPERATOR

$$\left.\frac{\Delta^2 f(x,\psi)}{\Delta\psi^2}\right|_{\psi=\psi'} \equiv 2\left\{\frac{Af(x,\psi_A) + Bf(x,\psi_B) + Cf(x,\psi_C)}{D}\right\} \qquad (B.4)$$

where:

for all cells except the wall cell and the last cell

$$A = k'$$

$$B = k$$

$$C = -(k + k')$$

$$D = k'k^2 + k'^2k$$

$$\psi_A = \psi' - k$$

$$\psi_B = \psi' + k'$$

$$\psi_C = \psi'$$

for the wall cell

$$A = (k' + k'')$$

$$B = -k'$$

$$C = -k''$$

$$D = k'^2(k' + k'') - k'(k' + k'')^2$$

$$\psi_A = \psi' + k'$$

$$\psi_B = \psi' + (k' + k'')$$

$$\psi_C = \psi'$$

for the last cell

$$A = (k + k')$$

$$B = -k$$

$$C = -k'$$

$$D = (k + k')\lambda^2 - (k + k')^2 k$$

$$\psi_A = \psi' - \lambda$$

$$\psi_B = \psi' - (k + k')$$

$$\psi_C = \psi'$$

DIFFERENCE EQUATIONS

Using the Δ operators defined above, Equations (45), (46), and (47) were approximated for the computational scheme as follows:

$$u(x+\Delta x) = u(x) + \Delta x \left\{ -\frac{1}{\rho u}\frac{dP}{dx} + \frac{\Delta}{\Delta\psi}\left[\nu\rho u\right]\frac{\Delta u}{\Delta\psi} + \nu\rho u\frac{\Delta^2 u}{\Delta\psi^2}\right\} \qquad (B.5)$$

$$F_j(x+\Delta x) = F_j(x) + \Delta x \left\{ \frac{1}{\rho u}\dot{w}_j + \frac{\Delta}{\Delta\psi}\left[\gamma_j\rho u\right]\frac{\Delta F_j}{\Delta\psi} + \gamma_j\rho u\frac{\Delta^2 F_j}{\Delta\psi^2}\right\} \qquad (B.6)$$

$$T(x+\Delta x) = T(x) + \Delta x\left\{\frac{1}{\rho C_p}\frac{dP}{dx} + \mu\rho u\left(\frac{\Delta u}{\Delta\psi}\right)^2\right.$$

$$- \frac{1}{\rho u C_p}\sum_i \dot{w}_i h_i + \frac{1}{C_p}\left[\sum_i \gamma_i \rho u \frac{\Delta F_i}{\Delta\psi}\frac{\Delta h_i}{\Delta\psi}\right]$$

$$\left. + \frac{1}{C_p}\left[\frac{\Delta}{\Delta\psi}(k\rho u)\frac{\Delta T}{\Delta\psi} + k\rho u\frac{\Delta^2 T}{\Delta\psi^2}\right]\right\} \qquad (B.7)$$

The pressure was fitted with an analytic curve, thus $\frac{dP}{dx}$ was taken from the derivative of the analytic curve.

Appendix C

Derivation of Boundary Conditions for F and F_2 Concentrations

There are two ways of approaching the derivation of the concentration boundary conditions. One way is purely analytic and will be discussed first; another way is to examine the analytic derivation in retrospect, this will be done second.

ANALYTIC

Since the no slip boundary condition for velocity is used, it would not seem a bad assumption to consider the region from the center of CELL 2 to the wall as being

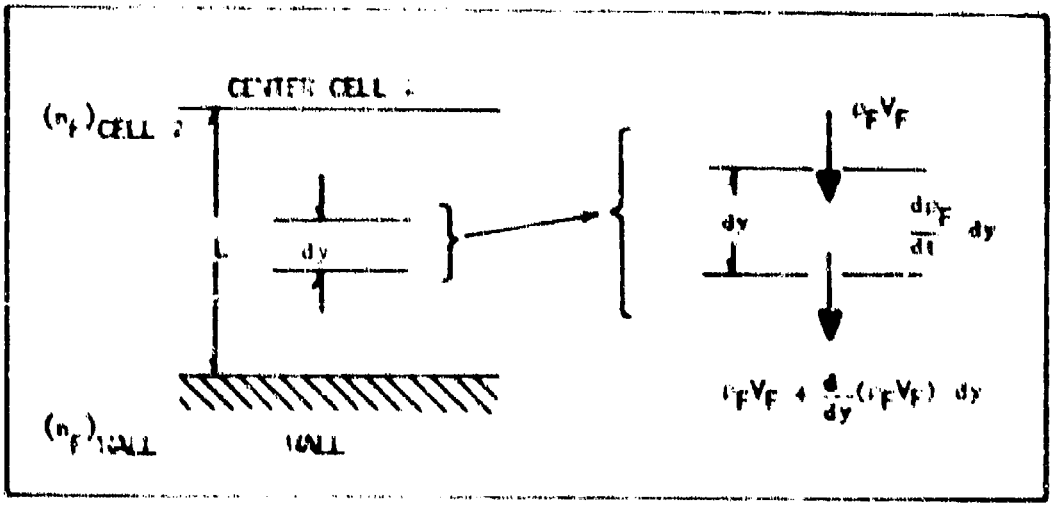

Figure C.1. Conservation Equations for Stagnant Cell

essentially stagnant. Further the horizontal concentration gradients are assumed to be negligible compared to the vertical. These assumptions lead to an analysis as shown in in Figure C.1.

The conservation of species equation in steady state is then written

$$\frac{d}{dy}\left(\rho_F v_F\right) = 0 \qquad \text{(C.1)}$$

By Fick's law

$$\rho_F v_F = -\rho_F \frac{dn_F}{dy} \qquad \text{(C.2)}$$

Thus the governing equation is

$$\frac{d}{dy}\left[\rho_F \frac{dn_F}{dy}\right] = 0 \qquad \text{(C.3)}$$

Integration yields

$$\rho_F \frac{dn_F}{dy} = A \qquad \text{(C.4)}$$

where A is a constant. In particular, at the catalytic wall, $y = L$, the steady state flux must be equal to the rate of recombination and attachment:

$$\text{Diffusive Flux} = 2\gamma\dot{N} \tag{C.5}$$

where the 2 accounts for the replacement of the wall atom detached by the recombination. This is necessary, to maintain the equilibrium wall concentration of F atoms. Thus

$$2\gamma n_F(L)\left(\frac{kT}{2\pi m_F}\right)^{1/2} = -D_F\frac{dn_F(L)}{dy} \tag{C.6}$$

And thus A must be

$$A = -2\gamma n_F(L)\left(\frac{kT}{2\pi m_F}\right)^{1/2} \tag{C.7}$$

We now have the differential equation

$$D_F\frac{dn_F}{dy} = -2\gamma n_F(L)\left(\frac{kT}{2\pi m_F}\right)^{1/2} \tag{C.8}$$

Assuming D_F is constant and integrating yields

$$n(y) = -2\frac{\gamma n_F(L)}{D_F}\left(\frac{kT}{2\pi m_F}\right)^{1/2} y + B \tag{C.9}$$

Since at $y = 0$ the concentration of F must be $(n_F)_{CELL\ 2}$, B must equal $(n_F)_{CELL\ 2}$. Thus we have

$$\frac{n_F(y)}{(n_F)_{CELL\ 2}} = -2\,\frac{n_F(L)}{(n_F)_{CELL\ 2}}\,\frac{\gamma\left(\frac{kT}{2\pi m_F}\right)^{1/2}}{D_F}\,y + 1 \qquad (C.10)$$

Finally since

$$\left.\frac{n_F(y)}{(n_F)_{CELL\ 2}}\right|_{y=L} = \frac{n_F(L)}{(n_F)_{CELL\ 2}} \qquad (C.11)$$

and realizing that $n_F(L) = (n_F)_{WALL}$ we have

$$\frac{(n_F)_{WALL}}{(n_F)_{CELL\ 2}} = \frac{1}{1 + \frac{2\gamma L}{D_F}\left(\frac{kT}{2\pi m_F}\right)^{1/2}} \qquad (C.12)$$

Similarly,

$$D_{F_2}\,\frac{dn_{F_2}(L)}{dy} = \frac{N}{4}\,\gamma n_F(L)\left(\frac{kT}{2\pi m_F}\right)^{1/2} \qquad (C.13)$$

since each recombination results in the creation of an F_2 molecule. Then in a similar manner to that used in getting Equation (C.8),

$$D_{F_2}\,\frac{dn_{F_2}}{dy} = \gamma n_F(L)\left(\frac{kT}{2\pi m_F}\right)^{1/2} \qquad (C.14)$$

and integration yields

$$n_{F_2}(y) = \frac{\gamma n_F(L)\left(\frac{kT}{2\pi m_F}\right)^{1/2}}{D_{F_2}}\,y + B \qquad (C.15)$$

Since, again, $n_{F_2}(y=0)$ is $(n_{F_2})_{CELL\ 2}$, F must equal $(n_{F_2})_{CELL\ 2}$. Thus knowing $(n_F)_{WALL}$ from Equation (C.12),

$$(n_{F_2})_{WALL} = \frac{(n_F)_{WALL}}{\nu_{F_2}} \gamma L \left(\frac{kT}{2\pi m_F}\right)^{1/2} + (n_{F_2})_{CELL\ 2} \qquad (C.16)$$

RETROSPECT

Starting from Equation (C.12)

$$\frac{(n_F)_{WALL}}{(n_F)_{CELL\ 2}} = \frac{1}{1 + \frac{2\gamma L}{\nu_F}\left(\frac{kT}{2\pi m_F}\right)^{1/2}} \qquad (C.17)$$

and rearranging it slightly yields:

$$-\nu_F \frac{\left[(n_F)_{WALL} - (n_F)_{CELL\ 2}\right]}{L} = 2\gamma (n_F)_{WALL} \left(\frac{kT}{2\pi m_F}\right)^{1/2} \qquad (C.18)$$

Equation (C.18) is the identical statement to assuming that the slope of the concentration at the wall is linear and approximating the derivative by

$$\frac{dn_F}{dy} \approx \frac{(n_F)_{WALL} - (n_F)_{CELL\ 2}}{L} \qquad (C.19)$$

Thus in retrospect one could have derived the boundary conditions for F and F_2 by merely assuming a linear profile at the wall.

Appendix D

Temperature and Pressure Dependence of the Fluorine Wall Recombination Coefficient

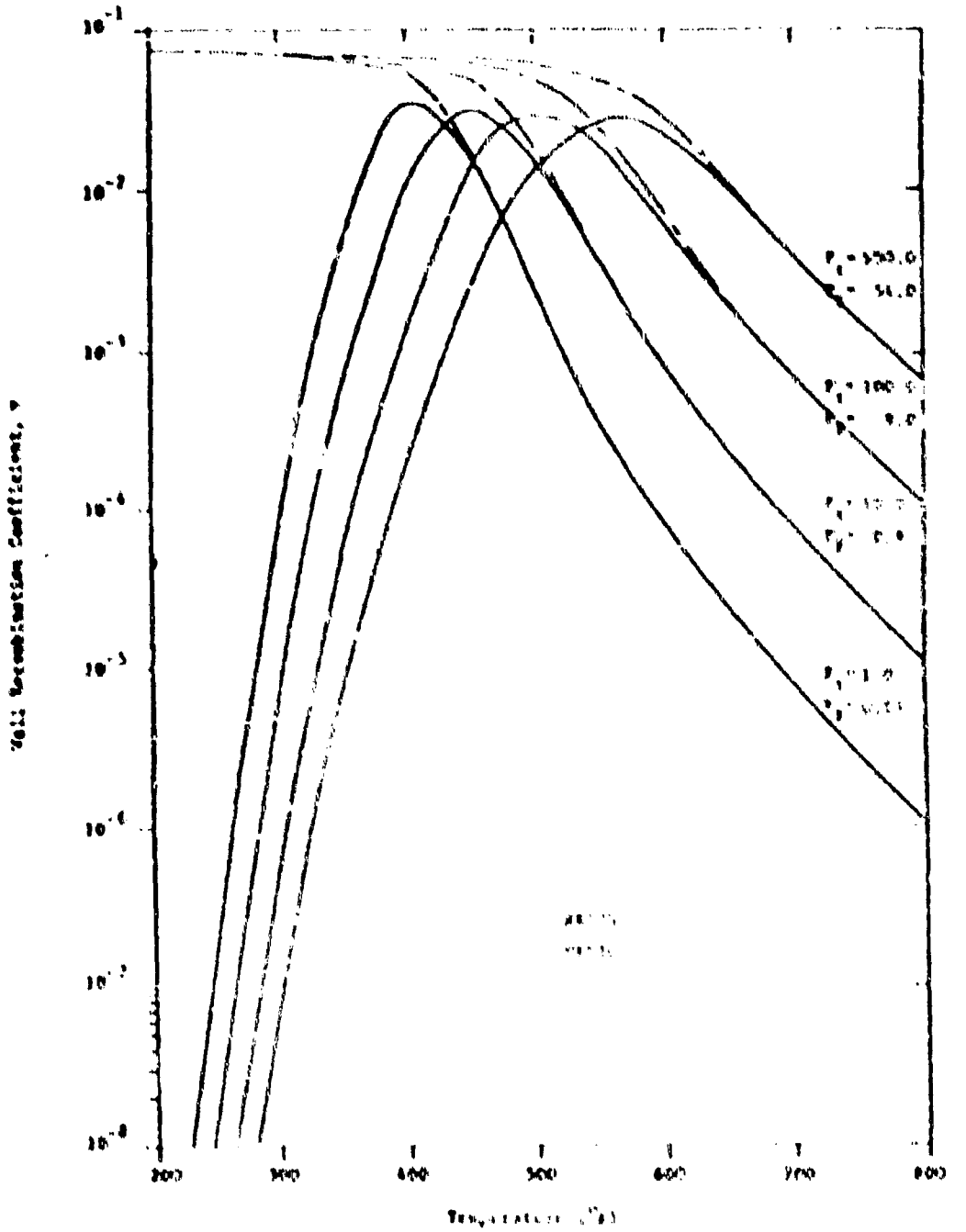

Figure D.1. Fluorine Wall Recombination Coefficient vs. Temperature for 90% Diluent Flows of ... and Helium with 90% Dissociation

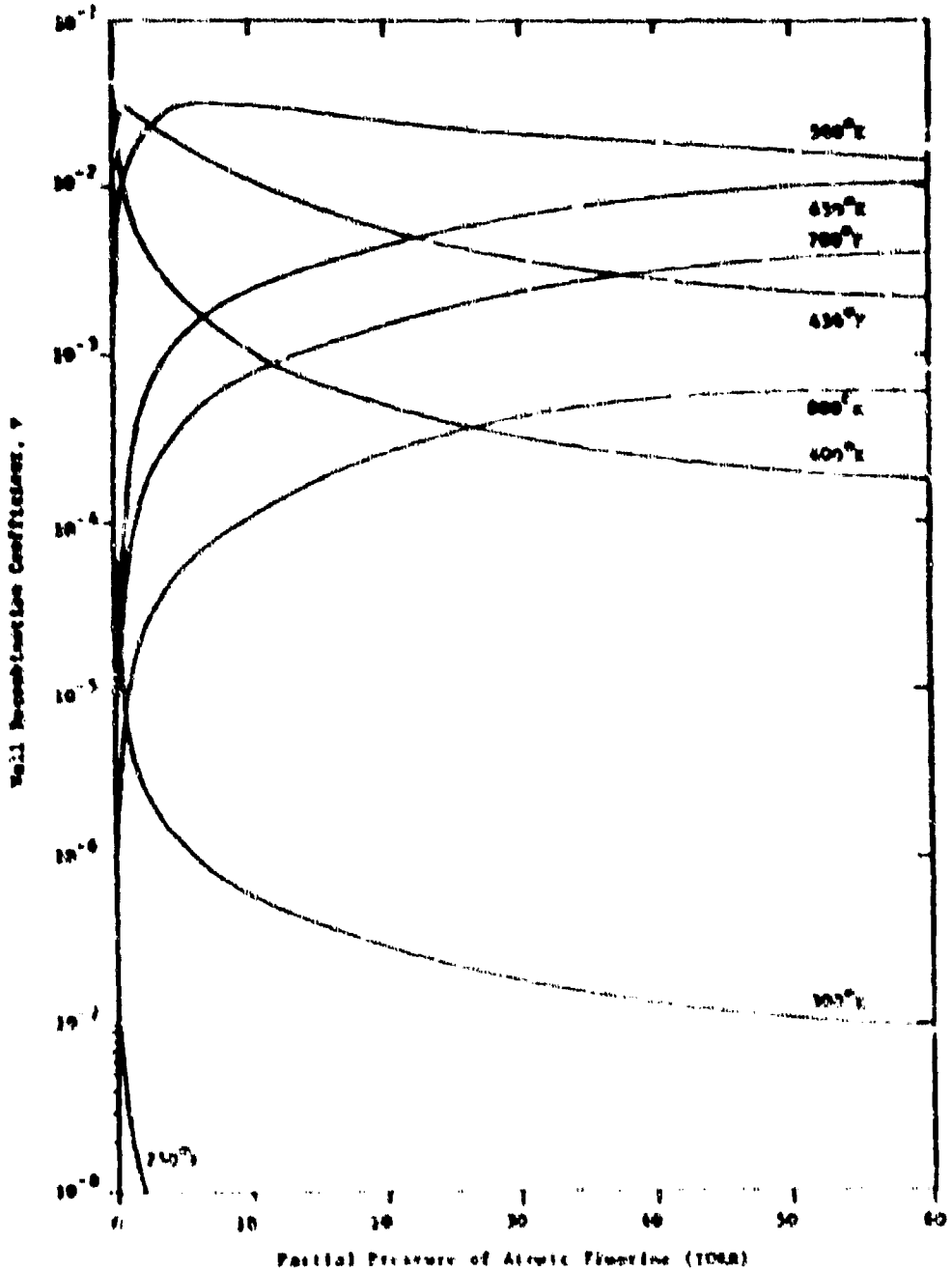

Figure D.2. Fluorine Recombination Coefficient vs. Partial Pressure of Atomic Fluorine for 90% Argon Diluent and 90% Fluorine Dissociation

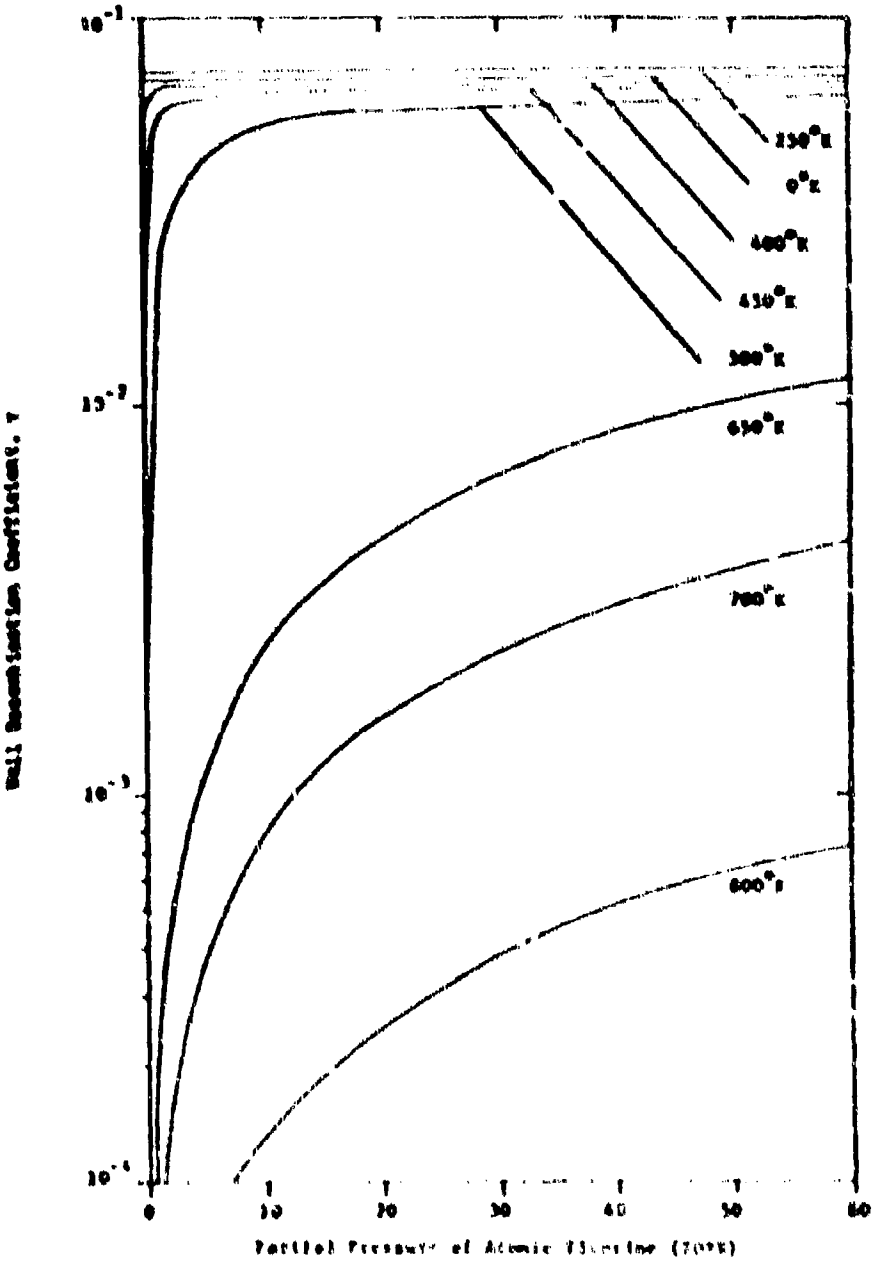

Figure D.3. Fluorine Recombination Coefficient vs. Partial Pressure of Atomic Fluorine for Helium Diluent

Vita

Captain Eric J. Jumper was born on 18 August 1946, in Washington, D. C. He graduated from Highlands High School, North Highlands, California in 1964, and attended the University of New Mexico where he received a Bachelor of Science Degree in Mechanical Engineering in June of 1968. Upon graduation he was commissioned a Second Lieutenant in the United States Air Force through the ROTC program. His first Air Force assignment was to the University of Wyoming for a Masters of Science Degree in Mechanical Engineering, graduating in August of 1969. From the University of Wyoming he was assigned to the 6570th Aerospace Medical Research Laboratory at Wright-Patterson AFB, Ohio, as a Branch Research Engineer. During his stay at the AeroMed Lab, Captain Jumper worked in such areas as work environments in zero-gravity, visual reconnaissance in flare light and haze, high altitude flight suit research, carbon monoxide toxicology, and circling line studies from fixed wing aircraft. In June 1972, he entered the PhD program at the Air Force Institute of Technology at Wright-Patterson AFB, Ohio. He completed all requirements for and was admitted to candidacy in January 1974. He is presently assigned to the Air Force Weapons Laboratory at Kirtland AFB, New Mexico.

Captain Jumper is married to the former Marjorie Lee Stanko of Albuquerque, New Mexico. Eric and Marge have two children: a son John, age 7, and a daughter Christine, age 6.

Permanent address: 7357 West Lane
Loomis, California 95650